Metaproteome analysis of the coral holobiont demonstrates algal symbiont dampening under thermal stress

Authors

Shrinivas Nandi[1,†], Timothy G. Stephens[2,†], Erin E. Chille[3], Samantha Goyen[4], Line K. Bay[4,*], Debashish Bhattacharya[2,*]

Affiliations

[1]Microbial Biology Graduate Program, Rutgers University, New Brunswick, New Jersey, 08901, USA

[2]Department of Biochemistry and Microbiology, Rutgers University, New Brunswick, New Jersey, 08901, USA

[3]Ecology and Evolution Graduate Program, Rutgers University, New Brunswick, New Jersey, 08901, USA

[4]Australian Institute of Marine Science, Townsville, Queensland, Australia

[†]These authors contributed equally.

[*]Corresponding authors: Debashish Bhattacharya, dbhattac@rutgers.edu; Line K. Bay, L.Bay@aims.gov.au

Abstract

The accelerating loss of coral reefs worldwide due to anthropogenic climate change has led to a myriad of studies aimed at understanding the basis of coral resilience to support reef conservation. Central to this effort is elucidating metabolic interactions between the cnidarian host and dinoflagellate algal symbionts, which has traditionally been challenging to do *in hospite*. Here, using data from four divergent coral species, we develop the first metaproteome model of thermal stress-based coral-algal dysbiosis. Our results demonstrate that thermal stress induces dampening of algal-symbiont metabolic pathways causing the host to shift its metabolism from symbiont maintenance to energy conservation. This putatively degrades symbiosome function, further degrading the symbiotic partnership. Although each coral host species we studied shows a distinct response to the stress regime, reflecting divergent evolutionary histories, symbiont dampening is consistently observed and comprises a major outcome of coral-algal dysbiosis. Our results also provide biomarkers for holobiont conservation.

Teaser

Coral algal symbionts show reduced protein abundance under thermal stress, disrupting host biology and leading to coral bleaching.

MAIN TEXT

Introduction

Stony corals (Scleractinia) thrive in oligotrophic waters due to their ability to form a symbiotic association with dinoflagellate algae in the family Symbiodiniaceae. The algal symbionts provide energy in the form of sugars, lipids, and other metabolites (*1*) . In exchange, corals provide Symbiodiniaceae with a stable, sheltered environment, inorganic carbon, and other essential nutrients (*2*). Under ambient conditions, coral species meet their energy needs from algal symbiont photosynthesis (*3*). The process by which corals lose their symbiotic algae upon exposure to stress is known as coral bleaching. During bleaching, some corals can sustain themselves for extended periods of time through heterotrophic feeding (*4*) . However, bleached corals are more susceptible to disease and may succumb to starvation if symbiosis is not reestablished (*5*) . The increase in mean global oceanic temperature, a result of anthropogenic climate change, has led to an increase in bleaching episodes and a significant decline in global coral populations.

Given its importance, the symbiosis between corals and Symbiodiniaceae has come under intense scrutiny. Under ambient conditions, corals maintain algal symbionts within their gastrodermal cells in specialized structures referred to as symbiosomes, which are related to lysosomes. Symbiosomes are acidified by the coral host using V-type ATPases, which improves photosynthetic performance (*6*, *7*). The host can control algal populations by limiting the supply of nitrogen, primarily ammonium and amino acids to the symbiosome (*8*, *9*). Stable isotope labeling experiments show that carbon-based metabolites (e.g., glucose, lipids, hexose sugars) are translocated from Symbiodiniaceae to the host *via* specialized transporters in the symbiosome membrane, including SWEETs (Sugars Will Eventually be Exported Transporters; (*10*)). These experiments also show that the host transfers ammonium to the symbiont *via* a rhesus channel protein (Rhp1) (*11*) and that coral carbonic anhydrases (*12*) and SLC4 (bicarbonate-transporter) proteins (*13*) play a role in the transfer of CO_2 to the symbiont. However, no mechanism has yet been identified for the transport of amino acids. The host and Symbiodiniaceae share the same amino acid pool, but the contributions of each partner are unknown. Nonetheless, the transfer of amino acids from the host to algal symbionts plays an essential role in preventing bleaching in heterotrophic corals. Stressed corals, which do not transfer amino acids to Symbiodiniaceae bleach more rapidly than those that maintain a steady supply of these metabolites, although the mode of transfer may differ, with some transferring amino acids, and others, ammonium (*14*, *15*).

Thermal stress leads to the production of excess reactive oxygen species (ROS) in the coral holobiont, which has been hypothesized as the primary cause of coral bleaching. Damaged photosystem II (PSII) in the endosymbiont was initially proposed as the source of this excess ROS (*16*–*18*). Another proposed source of ROS is the degradation of the electron transport chain in the host mitochondria, which was observed prior to any endosymbiont degradation (*19*). In addition, thermal stress studies performed in the dark have also observed the generation of ROS, suggesting at least one non-photosynthetic ROS source (*20*).

Until now, transcriptome data has been one of the primary tools for understanding and developing coral-algal dysbiosis models under thermal stress (*21*). However, recent studies of the rice coral *Montipora capitata* show that under a commonly used experimental design to thermally stress corals, changes in transcript expression are weakly

correlated (R^2 = 0.01-0.11) with accumulation of the encoded proteins (*22*). This result is unsurprising given existing knowledge from other eukaryotic model systems (*23–26*).

Whereas the utilization of proteomics to understand thermal stress in corals is nascent, similar analyses have been performed in other marine organisms. Thermal stress analyses in mussels, oysters, and marine algae have consistently found decreased protein abundances in energy metabolism, carbon fixation, and core metabolic pathways upon exposure to thermal stress (*27–30*). These studies have also described an increased abundance of proteins involved in enzymatic and non-enzymatic processes involved in detoxifying ROS (*27*). In particular, a shift from NADH-producing pathways to NADPH-producing pathways, which serves as the primary electron donor for various antioxidant enzymes, has been observed (*31*). While useful, few proteomic studies have been performed in marine symbiotic organisms (*32*, *33*), wherein the identity and abundance of proteins and metabolites detected may differ for each species *ex situ* versus in *in situ*, in the symbiotic state.

Here we use proteomic data to study the coral holobiont stress response. After creating a baseline understanding of the physiological and metabolic status of the coral holobiont, we generated metaproteomic (i.e., host and symbiont) data from *M. capitata* in Kāneʻohe Bay, Hawai□i. These lines of evidence were used to develop a working hypothesis of the role of protein regulation in coral-algal dysbiosis. Our data suggest that thermal stress induces "endosymbiont dampening", i.e., reduced protein abundance in algal endosymbiont central metabolic pathways, suggesting reduced metabolic activity. These results are consistent with existing dysbiosis models which have documented reduced photosynthetic efficiency of thermal stressed endosymbionts (*34*). Our results were tested and validated in data collected from three sympatric coral species (*Acropora hyacinthus*, *Porites lobata*, and *Stylophora pistillata*) from the Great Barrier Reef (GBR), Australia (**Fig. 1**). These three coral species have different levels of stress tolerance, *A. hyacinthus* and *S. pistillata* are sensitive to thermal stress, whereas *P. lobata* is relatively resilient (*35*, *36*). Although each coral host showed a distinct response to the stress regime, endosymbiont dampening was consistently observed. These data lead us to suggest that endosymbiont dampening is the major consequence of coral-algal dysbiosis and that the highly divergent responses observed in each coral species may result from different stress mitigation pathways that have evolved to enhance endosymbiont maintenance. Our results provide perspectives on coral-algal dysbiosis that can inform future work aimed at coral holobiont resilience and conservation.

Results

Using polar metabolomic data from the GBR corals, we investigated known thermal stress responsive metabolites to validate that the experimental design elicited the desired stress response. We focused on four dipeptides that were previously characterized in the Hawaiian samples (*37*) as having a strong positive response to thermal stress in *M. capitata*: lysine-glutamine (KQ), arginine-glutamine (RQ), arginine-alanine (RA), and arginine-valine (RV). We observed a significant (FC > 1.0 and p-value < 0.05) increase in dipeptide abundance in *A. hyacinthus* and *S. pistillata* (**Fig. 2, Table S1a**). *P. lobata* also showed increased abundance of these dipeptides, however fewer of these changes were statistically significant compared to the other two species.

We also assessed the abundance of other well-characterized antioxidant metabolites in these samples (*38*). Within each of the holobionts, we observed a different pattern of stress metabolite accumulation **(Table S1b)**. In *A. hyacinthus*, methionine, hypotaurine, and

CDP-choline showed significant increased accumulation at $TP1_G$ and/or $TP2_G$ (TP_G denotes timepoints from the GBR coral experiment). In the case of *S. pistillata*, we only observed a significant increase in phosphocholine abundance at $TP2_G$. In *P. lobata*, numerous antioxidant metabolites showed decreased abundance at $TP2_G$, including methionine, cystathione, and hypotaurine, however, none of these changes were statistically significant. Lastly, in all three GBR coral species, there was increased abundance of amino acids (**Table S1c**). In *A. hyacinthus*, at $TP1_G$ we observed an increased abundance of 9 amino acids (7 showed significant change) and at $TP2_G$ 9 amino acids had an increased abundance (4 showed significant change). In *S. pistillata* we observed increased abundance of 12 amino acids at $TP1_G$ (7 showed significant change). In *P. lobata* 7 amino acids had an increased abundance only at $TP2_G$ (4 showed significant change).

Endosymbiont physiology

For the Hawaiian *M. capitata* coral **(Figs S1A)**, change in endosymbiont cell density over the studied time points was assessed using color scores and housekeeping protein abundance (**Figs S1B** and **S1C**, respectively). These values serve as a rough proxy for endosymbiont cell density (not available for these samples) and suggest that significant endosymbiont cell loss was observed at $TP5_H$, but not $TP1_H$ or $TP3_H$ (TP_H denotes timepoints from the Hawaiian coral experiment).

For the three GBR corals, endosymbiont cell counts and PAM fluorometer measurements were taken for each of the samples collected at each time point (**Fig. S2**). Utilizing the $\log_2$ abundance of the endosymbiont counts, a statistically significant (adjusted *p*-value < 0.05) decrease in endosymbiont density was observed for *A. hyacinthus* at $TP1_G$ and $TP2_G$, (-1.32±0.36 and -1.22±0.30 respectively). Significant endosymbiont cell density loss was also observed in *S. pistillata* at $TP1_G$ (-0.88±0.27) ($TP2_G$ data not available). Lastly, significant symbiont loss was also observed in *P. lobata* at $TP2_G$ (-0.95± 0.28) (but not $TP1_G$) **(Fig. S2A**, **Table S2a)**. The PAM fluorometer data (**Fig. S2B**) are consistent with the endosymbiont cell density data, that is, there is a slight decrease in photosynthetic efficiency (i.e., F_v/Fm) at $TP1_G$ and $TP2_G$ for *A. hyacinthus* (-0.033±0.029 and -0.14±0.03 respectively), $TP1_G$ for *S. pistillata* (-0.13±0.03) ($TP2_G$ data not available), and at $TP2_G$ (-0.054 ± 0.016) (but not $TP1_G$) for *P. lobata*.

Profiling of endosymbionts

We utilized transcriptomic data developed in Williams et al. (*38*) to assess endosymbiont profiles in the Hawaiian coral *M. capitata.* Previous literature has shown this coral to be associated with both *Durusdinium* and *Cladocopium* algal endosymbionts (*39*, *40*). Our analysis supports this observation in our samples, with 85.95% of transcripts having a top BLAST hit to *Durusdinium trenchii* and 14.05% having a top BLAST hit to *Cladocopium goreaui*.

ITS2-based Symbiodiniaceae profiling of the three GBR coral species using the SymPortal platform shows that all samples associated exclusively with the Symbiodiniaceae species in the genus *Cladocopium* (except for one *P. lobata* replicate which had <1% relative abundance of *Gerakladium*). The three coral species had distinct major ITS2 type profiles which were C15-C15l-C15n-C15bb-C15.8 for all samples of *P. lobata*, C8/C1-C42.2 for all samples of *S. pistillata* and C3k/C3-C50a-C29-C21ab-C3b, C3/C3k-C50a-C3.10-C3gj-C3b and C3k-C50a-C3-C3ba-C50q-C3dq-C50f-C3a for all samples of *A. hyacinthus* (**Fig. S3, Table S2b**).

Hawaiian *M. capitata*

Endosymbiont response

A total of 562 algal proteins were identified in the proteome samples, 235 remained after low abundance filtering (**Table S3**). Whereas this filtering step focused our analysis on the more abundant proteins, we acknowledge the potential contribution of less abundant proteins in the coral stress response. At $TP1_H$, 46 algal proteins had differential accumulation (|FC| > 0.5), with five increasing in abundance (one had a significant *p*-value [< 0.05]) and 41 decreasing in abundance (7 had a significant *p*-value). At $TP3_H$, 192 algal proteins had differential accumulation, with five increasing in abundance (two had a significant *p*-value) and 187 decreasing in abundance (76 had a significant *p*-value). The proteins with decreased abundance had diverse functions, including carbohydrate metabolism (e.g., glycolysis, the TCA cycle), photosynthesis, and oxidative phosphorylation. Of the 235 algal proteins, 57 were putatively derived from *Cladodopium goreaui* strains and 178 from *Durusdinium trenchii* strains.

We observed a decrease in the accumulation of proteins in carbohydrate metabolism pathways in the endosymbiont. Of the 28 detected proteins in these pathways, all decreased in abundance at $TP3_H$ (14 had a significant *p*-value). Furthermore, decreased utilization of oxaloacetate to PEP *via* C-4 decarboxylation was observed. Oxidative phosphorylation [KEGG; ko00190] and photosynthesis [ko00195] pathways had relatively poor coverage in the proteome data. Three proteins from the endosymbiont oxidative phosphorylation pathway (F-ATPase [FC = -1.91, *p*-value = 0.013], V-ATPase [FC = -1.32, *p*-value = 0.010], and cytochrome c [FC = -1.11, *p*-value = 0.0035]) were detected after filtering, all had decreased abundance at $TP1_H$. We detected a total of six proteins in the photosynthesis pathway, arising from three genes: i.e., multiple copies of the same protein. All six copies of the proteins had a decreased abundance at $TP3_H$. The three detected proteins were PetH (FC = -1.32, *p*-value = 0.19), PsbV (FC = -1.83, *p*-value = 0.004), and PsbO (FC = -2.31, *p*-value = 0.0035), all of which showed a decreased abundance and two had significant *p*-values. Despite only detecting six of the endosymbiont photosystem proteins, algal carbon fixation [ko00710] had good coverage, with 11 out of 12 detected proteins showing a decreased abundance.

Host Response

A total of 4,904 *M. capitata* proteins were identified in all samples, of which 3,320 remained after low abundance filtering (**Table S4**). At $TP1_H$, 491 proteins had differential accumulation, with 279 proteins decreasing in abundance (58 had a significant *p*-value) and 212 proteins increasing in abundance (39 had a significant *p*-value). At $TP3_H$, 913 proteins had differential accumulation, with 514 decreasing in abundance (168 had a significant *p*-value) and 290 increasing in abundance (84 had a significant *p*-value).

A total of 41 proteins in host central carbohydrate metabolism pathways had differential accumulation values at $TP1_H$ or $TP3_H$, of which 22 had significant *p*-values. These proteins have diverse functions, including glycolysis/gluconeogenesis [ko00010], fructose mannose metabolism [ko00051], galactose metabolism [ko00052], the pentose phosphate pathway [ko00030], the TCA cycle [ko00020], glyoxylate and dicarboxylate metabolism [ko00630], methane metabolism [ko00680], nitrogen metabolism [ko00910], pyruvate metabolism [ko00620], and starch and sucrose metabolism [ko00500]. Eighteen proteins involved in oxidative phosphorylation [ko00190] were identified that had differential accumulation at either time point.

We identified 26 coral proteins with functions associated with the lysosome [ko04142] (i.e., putative symbiosome localized) with differential accumulation at either $TP1_H$ or $TP3_H$. Of these, V-type ATPases (VHA) play a crucial role in symbiosome acidification, which enhances algal photosynthetic efficiency. Four lysosome-associated VHA-encoding proteins were identified in the proteome data. Of these, two have an increased abundance at $TP1_H$ (ATPeV1H [K02144] and ATPeV0A [K02154]), whereas the other two [K02146, K03662] have FC values that were not differentially accumulated. The two VHAs with increased abundance at $TP1_H$ returned to ambient levels at $TP3_H$, indicating they may be involved in the initial response to thermal stress. In addition, we observed another five VHAs affiliated with oxidative phosphorylation [K02147, K02148, K02150, K02153, K03662] none of which showed differential accumulation. We observed a decreased abundance of several lysosomal proteins at $TP3_H$, some of which have been implicated in symbiosome function, including NPC2 (K13443; FC = -0.87, *p*-value = 0.079), cathepsin (CTSL; K01373; FC = -0.82, *p*-value = 0.039), (to a lesser degree) alpha-L-fucosidase (FUCA; K01206; FC = -0.40, *p*-value = 0.016), and others at $TP3_H$. We also identified three carbonic anhydrases, two are annotated as CA2 [K18245] and one as CA [K01672], which play an essential role in the carbon concentrating mechanism and in supplying the symbiosome. Two of these proteins (one copy of CA2; FC = -1.25, *p*-value = 0.03) and the one CA (FC = -0.73, *p*-value = 0.000383) had significant FC and *p*-value at $TP3_H$. Both proteins were had a decreased abundance at $TP3_H$.

At $TP3_H$, 16 proteins involved in fatty acid metabolism (from the fatty acid biosynthesis [ko00061], fatty acid elongation [ko00062], and fatty acid degradation [ko00071] pathways) had significant FC values, 14 of which had decreased abundance (four with a significant *p*-value) and two had increased abundance (both in the fatty acid degradation pathway).

Proteomic responses of the GBR coral endosymbionts

Potential Tank Effects

The accumulation pattern of proteins at $TP0_G$ before the treatment samples were subjected to high temperature allows for the analysis of potential tank effects in each of our study species (**Figs S4**). For the endosymbionts of *A. hyacinthus*, 571 proteins had differential accumulation (538 of which had an increased abundance), however, only 1 protein had a significant *p*-value. A similar trend was observed in the endosymbionts of *S. pistillata*, 370 proteins are differentially accumulated with only 68 having significant *p*-values. This effect was also detected in the endosymbionts of *P. lobata*, with 227 proteins differentially accumulated, 28 with significant *p*-values. We also analyzed the host proteome at $TP0_G$ (**Fig S5**). For *A. hyacinthus* 2,395 proteins were differentially accumulated (2,294 of which had an increased abundance), however only 22 proteins had significant *p*-values. For *S. pistillata*, 1,943 proteins were differentially accumulated, with only 187 significant proteins. Lastly, *P. lobata* had 1,381 differentially accumulated proteins, of which 266 were significant. Despite the large number of proteins with initial differential accumulation at $TP0_G$ the lack of statistical significance for many of them suggests that for each species the samples in the control and treatment tanks were relatively similar in terms of their starting proteome accumulation profiles. Although, *S. pistillata* and *P. lobata* did have some differentially accumulated proteins, suggesting that there were some starting tank effects for these two species.

A PCA of the host and endosymbiont proteomes from each species supports this result, with the *P. lobata* PCAs having the lowest variation explained by the first two PCs, suggesting that there was a significant amount of variation present between the samples from this species. Compared to the Hawaiian *M. capitata* samples, GBR species had much higher variation between their samples, PC1 in *M. capitata* were 86.0% and 50.4% endosymbiont and host respectively. Whereas in the three GBR species, the average PC1 score was 74.3% and 63%, respectively (**Fig. S6**).

Endosymbiont proteomic response to stress

After low abundance filtering, 849, 445, and 679 *A. hyacinthus, P. lobata*, and *S. pistillata* endosymbiont proteins remained, respectively (**Fig. S4**, **Tables S5-S7**). For *A. hyacinthus, P. lobata*, and *S. pistillata*, at $TP0_G$, 33, 135, and 339 had decreased abundance (0, 26, and 66 had a significant *p*-value) and 538, 92, and 31 had increased abundance (0, 2, and 2 had a significant *p*-value). At $TP1_G$, 457, 201, and 251 had a decreased abundance (62, 35, and 138 had a significant *p*-value) and 34, 61, and 35 had an increased abundance (3, 5, and 2 had a significant *p*-value). Finally, for *A. hyacinthus* and *P. lobata* at $TP2_G$, 683 and 183 had a decreased abundance (403 and 54 had a significant *p*-value) and 15 and 115 had an increased abundance (0 and 20 had a significant *p*-value). It should be noted that many of the differentially accumulated endosymbiont proteins are multicopy, with many having the same accumulation values. Regardless, the large number of proteins with decreased abundance under high temperature, particularly at later time points, is congruent with the endosymbiont dampening observed in the Hawaiian *M. capitata* proteomic data.

Pathways of interest in GBR endosymbionts

The implicated pathways (i.e., amino acid biosynthesis, carbohydrate metabolism, fatty acid metabolism, oxidative phosphorylation, photosynthesis and carbon fixation function), identified as being responsive to high-temperature treatment in endosymbionts of the Hawaiian *M. capitata* (**Table S8**), were analyzed using the GBR data to determine if consistent patterns were observed in these species.

At $TP1_G$, we identified numerous endosymbiont proteins in our metabolic pathways of interest in *A. hyacinthus, P. lobata*, and *S. pistillata* that showed decreased abundance: i.e., FC < -0.5, (43.6%, 58.7%, and 43.8%, respectively; **Figs 3A** and **S4**), with fewer (7.6%, 3.9%, and 3.5%) having increased abundance. Furthermore, at $TP2_G$, 91.5% of target pathway proteins in *A. hyacinthus* endosymbionts had decreased abundance, with many more having a significant *p*-value at this time point than at $TP1_G$, suggesting that this affect increased the longer the coral was under thermal stress (45 $TP1_G$ vs. 131 at $TP2_G$). Lastly, even in *P. lobata* we observed that 49.0% of endosymbiont target pathway proteins showed a decreased accumulation. For *S. pistillata* we observed a decreased accumulation of endosymbiont proteins across all time points, including $TP0_G$ (prior to thermal stress), suggesting a potential tank effect. However, the lack of any statistical significance at $TP0_G$ when compared to $TP1_G$ suggests significant proteomic dampening upon exposure to thermal stress (5 at $TP0_G$ vs. 54 at $TP1_G$). A similar response was observed in the endosymbionts of *P. lobata* (8 at $TP0_G$ vs. 16 at $TP1_G$).

There was a decrease in the utilization of endosymbiont photosynthesis pathways in all three coral species during the thermal stress treatment (**Table S8, Fig. S7**). Ten photosynthesis related proteins had decreased abundance in all three coral endosymbiont datasets, PetH (K02641; ferredoxin-$NADP^+$ reductase), which was statistically significant in *A. hyacinthus* at $TP2_G$. Photosystem (PS) proteins PsbO [K02716] and PsaD [K02692]

also showed decreased abundance and statistical significance across all three datasets. Lastly, PsbD [K02706], required for maintaining PSII stability, showed decreased abundance at $TP1_G$ in all three datasets [*P. lobata* = - 0.60, *S. pistillata* = -0.37, and *A. hyacinthus* = -1.04].

We also studied the impacts of thermal stress on endosymbiont carbon fixation pathways (**Fig. S8**). Six proteins were shared in a common response across the endosymbionts of all three species upon exposure to thermal stress. One of these, FbaA [fructose-bisphosphate aldolase; *S. pistillata* = -1.78 ($TP1_G$), *A. hyacinthus* = -1.78 ($TP2_G$), and *P. lobata* = -3.82 ($TP2_G$)], plays a fundamental role in both glycolysis and carbon fixation by catalyzing the conversion of fructose 1,6 bisphosphate to glyceraldehyde 3 phosphate and dihodroxy acetone. A second protein, PPC, phosphoenolpyruvate carboxylase, also followed a similar pattern of decreasing abundance across all three GBR coral endosymbionts. Other proteins that followed a consistent decreasing trend across the endosymbionts in the three corals were, GAPDH, RbcL, sedoheptulose bisphosphatase, and TktA.

Proteomic responses of the GBR coral hosts

Overall proteome responses

A total of 3,060, 3,187, and 1,903 host proteins were detected in the raw proteomic data from *A. hyacinthus, P. lobata*, and *S. pistillata*, respectively. After filtering, 2,839, 3,061, and 1,798 host proteins remained, respectively (**Fig. S5**; **Tables S9-S11**). For *A. hyacinthus, P. lobata*, and *S. pistillata* at $TP0_G$, 2,294, 730, and 136 host proteins had an increased abundance (19, 95, and 4 had a significant *p*-value) and 101, 651, and 1003 had a decreased abundance (3, 166, and 183 had a significant *p*-value). At $TP1_G$ 210, 421, and 313 proteins had an increased abundance (42, 36, and 127 had a significant *p*-value) and 1,409, 985, and 376 had a decreased abundance (338, 174, and 108 had a significant p-value). Finally, at $TP2_G$ for *A. hyacinthus* and *P. lobata* 442 and 554 proteins had an increased in abundance (115 and 152 had a significant *p*-value) and 692 and 1,251 had a decreased abundance (191 and 464 had a significant *p*-value) (**Fig. 3B**).

Accumulation pattern of pathways implicated in the coral thermal stress response

Based on the accumulation patterns observed in the *M. capitata* host proteome, we identified metabolic pathways (**Table S12**) that are responsive to thermal stress and assessed their accumulation patterns in the three GBR coral species. We observed that *A. hyacinthus* has the strongest initial response to the apparent dampening of the endosymbiont proteome; 53.4% and 16.2% of host proteins involved in the target pathways decreasing in abundance at $TP1_G$ and $TP2_G$ (respectively). In contrast, 29.2% of *P. lobata* host proteins decreased in abundance at $TP1_G$, 9.2% had increased abundance. At $TP2_G$, 34.6% of *P. lobata* proteins decreased in abundance and 16.8% showed an increase in abundance. For *S. pistillata*, 13.4% of host proteins decreased in abundance at $TP1_G$, 7.6% showed an increase in abundance.

Host-derived ROS-response proteins

The seepage of reactive oxidative species (ROS) into the coral host has been posited to be a cause of coral bleaching. Preliminary results from *M. capitata* showed little increase in abundance of ROS response proteins: e.g., superoxide dismutase (SOD) and catalases (**Table S4**). In *A. hyacinthus* at $TP1_G$, we observe decreased abundance of all catalases and SOD proteins, with no differential accumulation at $TP2_G$. In *P. lobata*, differential accumulation was not observed at $TP1_G$, however at $TP2_G$, of the four detected ROS response proteins, only one catalase had increased abundance, though not significant (FC

= 1.41, *p*-value = 0.07). Lastly, in *S. pistillata*, at $TP1_G$ only one catalase showed increased abundance (FC = 0.65, *p*-value = 0.35), however, SOD1 had decreased abundance (FC = -0.47, *p*-value = 0.23).

Whereas enzymatic pathways for ROS detoxification are vital, several studies have shown the necessary role of non-enzymatic pathways in this process in marine organisms (*27*). One non-enzymatic pathway responsive to ROS stress is the proteasome. In *A. hyacinthus*, *P. lobata*, and *S. pistillata* we detected 34, 38, and 31 proteins, respectively, that are associated with the proteasome (**Table S12**). At $TP1_G$ 3, 3, and 4 proteins had an increased abundance (0, 0, 1 had a significant *p*-value), whereas 17, 13, and 3 proteins had a decreased abundance (3, 3, and 1 had a significant *p*-value), respectively. Furthermore, in *A. hyacinthus* and *P. lobata* at $TP2_G$, 3 and 5 proteins had an increased abundance in (0 and 1 had a significant *p*-value), and 5 and 14 proteins had a decreased abundance (2 and 5 had a significant *p*-value), respectively.

The glutathione pathway also plays a vital role in detoxifying ROS. Using polar metabolomics, we were able to assess the relative abundance of glutathione in all three coral species. No significant shifts in glutathione abundance were detected in any of the three species, excluding *A. hyacinthus* at $TP1_G$ with a FC of 1.33 (*p*-value = 0.08). We also assessed enzymes involved in glutathione induced ROS detoxification, namely, glutathione reductase (GSR), glutathione synthetase (GSS), glutathione peroxidase (GPx), and glutathione S-transferase (GST) (**Tables S9-S11**). In *A. hyacinthus*, we detected 2, 2, 1, and 4 copies of GSR, GSS, GPx, and GST (**Table S9**), respectively. At TP1 one copy of GSR (FC = -0.54, *p*-value = 0.19) and one copy of GSS (FC = -0.84, *p*-value = 0.02) had a decreased abundance. GPx had decreased abundance at both $TP1_G$ and $TP2_G$ (FC = -0.97, *p*-value = 0.09; FC = -0.83, *p*-value = 0.09, respectively). Two copies of GST had a decreased abundance at both $TP1_G$ and $TP2_G$, of which only one copy was statistically significant (FC = -1.45, *p*-value = 0.004; FC = -0.50, *p*-value = 0.033, respectively). In *P. lobata* we detected 1, 1, 2, and 6 copies of GSR, GSS, GPx, and GST, respectively (**Table S10**). No shifts were observed in GSR. Whereas GSS had a decreased abundance at both $TP1_G$ and $TP2_G$ (FC = -0.55, *p*-value = 0.041; FC = -0.84, *p*-value = 0.17, respectively). Two copies of GPx had a decreased abundance at only $TP2_G$, however neither were statistically significant. At $TP1_G$ 1 copy of GST had an increased abundance and 1 had a decreased abundance, neither were statistically significant. At TP2, one copy had a decreased abundance, and 4 copies had an increased abundance, but none were statistically significant. Lastly, in *S. pistillata* we detected 1, 1, 0, and 4 copies, of GSR, GSS, GPx, and GST, respectively (**Table S11**). There were no shifts detected in both GSR and GSS. Only one copy of GST had a decreased abundance at $TP1_G$ (FC = -1.55, *p*-value = 0.36).

We also assessed protein abundance in the pentose phosphate pathway (PPP). In *A. hyacinthus*, *P. lobata*, and *S. pistillata*, we detected 13, 14, and 10 proteins, respectively, that are involved in the PPP. At $TP1_G$ 1, 0, and 0 proteins had an increased abundance of which none are significant, and 7, 2, and 4 proteins had a decreased abundance (2, 0, and 1 had a significant *p*-value). At $TP2_G$ in *A. hyacinthus* and *P. lobata*, 0 and 3 proteins had an increased abundance (0 and 1 had a significant *p*-value), and 1 and 3 proteins had a decreased abundance (0 and 1 had a significant *p*-value).

Host symbiosome maintenance

The transfer of substrates between the host and endosymbiont is critical for maintaining a stable symbiosis. The vesicle transport protein SEC22 showed decreased abundance in *A. hyacinthus* ($TP1_G$ and $TP2_G$) and *P. lobata* (at $TP1_G$) (**Table S4**). Vtype ATPases play a fundamental role in maintaining the endosymbiont photosynthetic efficiency by acidifying the symbiosome. We identified two Vtype ATPases in *S. pistillata*, however, many more were detected in *A. hyacinthus* and *P. lobata*. In *A. hyacinthus*, all seven Vtype ATPases showed decreased abundance at $TP1_G$, and two of these, ATPeV1D and ATPeV1E, showed decreased abundance at $TP2_G$. In *P. lobata*, in contrast to *A. hyacinthus*, the majority of Vtype ATPase proteins had no differential accumulation, however two proteins, ATPeV1C and ATPeV1F had decreased abundance at $TP1_G$ and $TP2_G$ (**Fig. S9**).

Discussion

Dipeptides markers of coral stress

Much effort has been expended by coral researchers in studying differences in the accumulation pattern of cDNAs, proteins, and metabolites that may be indicative of thermal stress prior to bleaching to aid conservation efforts (*33*, *37*, *41*) .Whereas relatively few studies have focused on coral metabolite biomarkers of stress, canonical animal stress-responsive metabolites, such as methionine, methionine sulfoxide, CDP-choline, and taurine have been shown to be promising targets in corals (*37*). In our study, we focused primarily on dipeptides because they are some of the most robust markers of coral stress. In a previous analysis of the Hawaiian *M. capitata* data used in this research, we identified four dipeptides that are candidate stress biomarkers (RQ, KQ, RA, and RV) (*37*). These dipeptides are likely to be of host animal provenance because they are produced by aposymbiotic *Aiptasia* (non-biomineralizing cnidarian sister lineage to corals). Importantly, dipeptide abundance increases in symbiotic *Aiptasia*, suggesting a link to the presence of algal symbionts (*37*). We find that dipeptides, in particular arginine-glutamine and lysine-glutamine, show a similar pattern of accumulation under thermal stress for the GBR corals (at $TP2_G$) as they did for Hawaiian species, consistent with our physiological measurements. As was observed for *M. capitata* (*37*, *42*) ,different dipeptides show divergent accumulation patterns in each of the three GBR species, suggesting, that each has a different response to heat stress. Furthermore, the presence of dipeptides in the GBR species indicate that corals are adequately stressed, supporting the validity of our experimental design and the comparability of the two experiments. Canonical stress metabolite biomarkers, such as CDP-choline and taurine had differing accumulation patterns across the GBR species.

Lastly, we observe an increased accumulation of numerous amino acids in all three GBR coral holobionts assessed (see **Table S1c**). We hypothesize that free amino acids may result from protein degradation and are subsequently funneled into the TCA cycle to sustain host metabolism. This idea, however, needs validation using stable isotope assays to identify the producers of these amino acids and the potential pathways involved.

M. capitata holobiont thermal stress response

Using the Hawaiian *M. capitata* metaproteome data, we generated a working hypothesis for the role of protein regulation in stress-induced coral-algal dysbiosis (**Fig. 4**). Under ambient conditions, the coral host facilitates Symbiodiniaceae photosynthesis by supplying CO_2 *via* VHA-mediated acidification of the symbiosome. In exchange, the algal endosymbionts provide the coral with photosynthesis-derived compounds, such as glucose and acetate (*1*). The host also supplies Symbiodiniaceae with nitrogen, either in the form of ammonium or amino acids, which may control endosymbiont populations by creating a

nitrogen replete or depleted state to control replication (*8, 9, 15*). Under thermal stress, endosymbionts may experience photosystem damage, leading to reduced photosynthetic capacity (*34*). The algae show decreased abundance of proteins involved in carbon fixation and central metabolic pathways, that may act to mitigate metabolic dysfunction. This response putatively leads to diminished delivery of photosynthates to the coral host, which has been well characterized in existing literature (*43*). Whereas some differential gene expression studies have found a mixed response in the endosymbiont, our meta-proteome further elucidates the extent of endosymbiont proteomic dampening, evidenced by an overwhelming decrease in protein abundances in numerous metabolic pathways (**Fig 4**). These are exemplified by decreased accumulation of proteins involved in photosynthesis, carbon fixation, oxidative phosphorylation, and carbohydrate metabolism.

We suggest that initially, likely in response to the reduction in endosymbiont photosynthate production, the host increases the supply of bicarbonate to the algae by further acidifying the symbiosome (i.e., increase in VHA abundance at $TP1_H$). During this stage, the host utilizes its stored energy reserves (e.g., sucrose, maltose, starch) to sustain central metabolism and continued acidification of the symbiosome (i.e., increased accumulation of starch and sucrose metabolism proteins and $TP1_H$). Eventually, the host halts this process (seen by the decrease in VHA abundance at $TP3_H$) and decreases the abundance of many lysosomal proteins potentially involved in symbiosome maintenance.

Although out of the scope of the experiment, based on existing literature we hypothesize that the host after $TP3_H$ reduces provisioning of nitrogen in the form of ammonium and amino acids to the symbiosome to prevent wasting nutrients on an unproductive symbiont. At this stage, we hypothesize that the coral host utilizes lipids, fatty acids, and amino acids to sustain itself, as has been previously studied in coral species (*9*). These changes likely result in a positive feedback loop: i.e., the initial decrease in abundance of proteins involved in endosymbiont metabolism reduces photosynthate transport to the host, which results in the host conserving energy by reducing accumulation of bicarbonate and nitrogen in the symbiosome, further reducing endosymbiont metabolism and photosynthate transport. These interactions are likely to be the final shift in host metabolism before the onset of bleaching (which we observe at $TP5_H$ in our experiment). However, a more long-term stress experiment with finer-scale sampling is required to validate this hypothesis.

Thermal stress response in the GBR corals

To test the working hypothesis developed in *M. capitata* we analyzed meta-proteome data from three sympatric GBR coral species. Whereas we observe some tank effects at $TP0_G$, particularly for *P. lobata*, we do not expect that these artefacts will significantly impact interpretation of our results given that our analysis focuses on the change in overall protein accumulation patterns across the time points, and not on the change at each time points in isolation. Given the results, we propose that algal dampening underpins the unidirectional decrease in protein abundance, often from a limited number of pathways in the endosymbiont, observed at varying degree across all the examined coral species (**Fig. 3A)**.

Endosymbiont dampening in corals

Upon exposure to thermal stress, we observed endosymbiont dampening in all three GBR coral species, consistent with the model developed in *M. capitata*. The protein accumulation pattern of *A. hyacinthus* was nearly identical to that of *M. capitata*, that is,

we observed a shift towards endosymbiont dampening at $TP1_G$, which was exacerbated at $TP2_G$ due to longer exposure to thermal stress. A very similar result was observed in metabolism-related proteins in endosymbionts of the coral *S. pistillata* (**Fig. 3A**), however, because these corals "bailed out" (i.e., underwent rapid tissue loss) (*44*), before $TP2_G$, we cannot fully address this response under prolonged thermal stress. Lastly, in the endosymbionts of *P. lobata*, whereas strong tank effects were observed at $TP0_G$, this effect did not change even after inducing thermal stress. Given this tank effect, we suggest caution when interpreting these results. However, given that we observe the expected decline in endosymbiont photosynthetic efficiency (**Fig. S2**) and an increase in known coral stress metabolite biomarkers (**Fig. 2**) in *P. lobata*, we conclude that the samples underwent thermal stress. Furthermore, the fact that endosymbiont proteins started in a state of reduced abundance at $TP0_G$ and remained so for the remainder of the experiment, suggests that dampening may be a general algal stress response (in this case, potentially due to being relocated to tanks).

The decreased abundance of canonical photosynthesis-related proteins in all three corals demonstrates lower algal photosynthetic activity. PetH, which catalyzes the terminal step in PSI-associated electron transport (i.e., converting $NADP^+$ and H^+ into NADPH) (**Fig. S7**) showed decreased abundance in the endosymbionts of all three coral endosymbionts. Furthermore, PsbD (D2 polypeptide), which is needed to maintain the stability of PSII, also showed decreased abundance at $TP1_G$ in all endosymbiont populations. This result was supported by the observed reduction in photosynthetic efficiency (PAM fluorometry; **Fig. S2**) in endosymbionts of the three coral species. Finally, the endosymbiont composition varied across the four coral species, demonstrating that this response (algal dampening) is consistent regardless of the genotype of the endosymbiont.

This dampening of core algal metabolic pathways is consistent with other proteomic studies on the impacts of thermal stress in marine species (*27*, *29–31*). For example, in the foraminifera *Amphistegina gibbosa*, which forms an endosymbiosis with diatoms, a similar reduction in abundance of proteins involved in central metabolic pathways is observed (*32*). In diatoms, whereas energy metabolism, including photosynthesis and carbon fixation showed decreased abundance, other pathways had increased protein abundance. In this study, we observe a complete dampening of the algal proteome across the coral species that were studied, regardless of composition of the algal endosymbiont population. This result suggests that coral endosymbionts are undergoing a similar process to what has been described in other algae under thermal stress, albeit in a fashion that reflects coral holobiont biology.

Endosymbiont impact on host responses

Our working hypothesis of the progression of coral-algal dysbiosis in *M. capitata* suggests that upon thermal stress, algal symbionts experience proteomic dampening, and the host initially attempts to restore symbiont activity. If the stress continues, the host curtails support of symbiosomes, ultimately leading to algal expulsion. Testing this hypothesis using GBR corals supports the model. However, the proteomic response of each host cnidarian to thermal stress and endosymbiont dampening has diverged (**Fig. 5**).

Corals rely primarily on algal symbionts to meet their metabolic needs therefore symbiont dampening has a drastic effect on overall holobiont fitness. The lack of photosynthate transfer by algae leads to an initial reduction in the abundance of many host proteins,

suggesting reduced metabolic activity, as observed at $TP1_G$ in *A. hyacinthus.* A slight recovery in the host proteome was observed at $TP2_G$, with many proteins still having a decreased abundance. We therefore characterize *A. hyacinthus* as a stress-sensitive phenotype, owing to the initial reduction in protein abundance upon experiencing algal symbiont proteomic dampening. The sensitive phenotype of the *Acropora* genus has been documented in the literature (*36*) and consistent with our meta-proteomic data. In contrast, the *S. pistillata* coral host "bailed out" upon exposure to thermal stress and algal proteomic dampening, which is a common response for this species (*44*). Lastly, *P. lobata*, which did show tank effects at the start of the experiment had a very similar overall response to thermal stress and endosymbiont dampening as *M. capitata*: i.e., no drastic shifts in the host proteome. This stress resilience phenotype is consistent with the field observations of the *Porites* genus and *M. capitata* (*45*) . Therefore, of the four coral species investigated in this study, we divide them into three distinct stress response phenomes (i.e., sensitive, bail-out, resilient; **Fig. 5**), all consistent with their known ecological responses in other studies.

Shared host responses across all coral species

Reactive oxygen species (ROS) have been suggested as the primary trigger for coral bleaching: i.e., the hypothesis being that ROS production by the endosymbiont during thermal stress seeps into the host cytosol, triggering endosymbiont expulsion (*16*). ROS can be detoxified using enzymatic and non-enzymatic pathways. Upon exposure to thermal stress, we did not observe a significant increase in ROS detoxification protein abundance in any of the coral species, except *S. pistillata*, which showed increased abundance for one of four SOD proteins. We also investigated non-enzymatic pathways for ROS detoxification that are thermal stress responsive in other marine organisms. Previous studies demonstrate that attenuation of proteasome subunit abundance may prolong the lifespan of proteins. Furthermore, oxidative stress proteins persist longer in response to a decrease in the proteasome. Within our datasets, we observed a clear decrease in the abundance of proteasome proteins across the three GBR corals upon exposure to thermal stress. We also assessed glutathione metabolism which is a key mechanism involved in ROS detoxification. Within the metabolome, glutathione was maintained stable levels across the three species, with only a short-term increase in abundance at $TP1_G$ in *A. hyacinthus.* However, enzymes involved in glutathione metabolism (GSR, GPx, GSS, and GST) had divergent responses upon exposure to stress. In *A. hyacinthus*, these enzymes had decreased abundance upon exposure to stress, whereas in *P. lobata*, a mixed response was observed, with GST proteins, encoded by five different genes in this species, showing increased abundance for four, and decreased abundance for one (**Table S11**). A minimal response was observed in *S. pistillata*.

NADPH serves as an electron donor for ROS detoxifying enzymes, such as GSR. Previous studies in marine organisms have shown a shift towards NADPH-producing pathways under thermal stress, primarily the pentose phosphate pathway. However, in our study, proteins associated with the pentose phosphate pathway had a decreased abundance in *A. hyacinthus* and in *S. pistillata*. A mixed response was observed in *P. lobata*, which is the more highly resilient of the three species we studied from the GBR. The apparent lack of a consistent protein level response to ROS is intriguing, however, additional research is needed to elucidate the connection between the proteome and ROS production and detoxification in coral holobionts. Lastly, the decrease of Vtype ATPases and other phagosomal and lysosomal proteins in all studied coral species supports our hypothesis

that the host reduces its energy expenditure on symbiosome maintenance due to endosymbiont dampening.

Materials and Methods

Hawaiian *M. capitata* data

Experimental set-up

The metaproteomic datasets analyzed in this study were generated from samples collected as part of a mesocosm experiment that has previously been described in detail (*22*, *38*). In brief, samples from one genotype (i.e., same colony) of *M. capitata* (**Fig. 1A**; MC- 289) coral was collected Kāneʻohe Bay, Oahu, Hawai□i. The colony was fragmented into 30 pieces (nubbins) and randomly allocated to one of six indoor experimental tanks (three treatment and three control) which had flow-through systems that took in water directly from the bay. After a five-day acclimation period at ambient temperature (~27°C), the temperature of the treatment tanks was increased by ~0.4°C every two days for nine days until the target of 30.5-31°C (i.e., high) was reached, and the tanks were kept at this temperature for the 16-day treatment period. The ambient tanks were held at ~27°C (i.e., ambient) for the entire experiment. Samples (n = 3 replicate nubbins/condition/time point) were collected at five time points (TP_H denotes Hawaiian samples) during the treatment phase of the experiment, however, only samples collected at $TP1_H$ (after ramp-up), $TP3_H$ (bleaching first observed; 13 days after $TP1_H$), and $TP5_H$ (last day of treatment; 15 days after $TP1_H$) were used for proteomic analysis because they represent the most critical stages of the experiment. Color scores, a non-destructive measurement utilized as a measure of coral bleaching, were noted for each of the available nubbins at each time point. Three nubbins were also collected from the same coral colonies in Kāneʻohe Bay (i.e., field samples) and included in the downstream analysis. Proteomic data were generated from the same genotype (MC-289), using 2 out of the 3 replicate nubbins collected at each condition and time point.

Endosymbiont typing from RNA-seq data

The composition of the algal endosymbionts was assessed in the coral samples using the available RNA-seq data published by Williams et al. 2021(*38*) (BioProject: PRJNA694677). Reads were trimmed for adapters and low quality regions using Trimmomatic v0.38 (“ILLUMINACLIP:adapters.fa:2:30:10 SLIDINGWINDOW:4:5 LEADING:5 TRAILING:5 MINLEN:25”) (*46*) aligned to the *M. capitata* (version 1) (*47*) genome assembly using HISAT2 v2.2.1 (*48*) and had unmapped read pairs extracted using samtools v1.11 ("view -f12”) and the bbmaps “repair.sh” script. These unmapped (non-host, putatively algal) reads were assembled into a single transcriptome using Trinity v2.11.0 (“--SS_lib_type RF”) (*49*). The resulting transcripts were compared against the predicted proteins from *M. capitata* V3 (version 3) (*50*), *Durusdinium trenchii* CCMP2556 (*51*), and *Cladocopium goreaui* (*52*) using BLASTX (v2.13.0). The resulting hits were filtered, keeping the best hit per transcript query, removing hits with < 50% query or subject coverage, and kept those that had an *e-value* < 1E-05. The proportion of transcript with top hits to each of the algal proteomes was used as a proxy for the endosymbiont composition across the samples and to guide proteomic database construction.

Proteome data production

The proteomic data (available from MassIVE under the ID MSV000088443; see Williams et al. (*22*) for a detailed description of sample extraction and processing) were reanalyzed with Proteome Discover v2.4.0.305 (ThermoFisher). In brief, protein concentrations were

measured using the Pierce 660-nm Protein Assay. 40µg of each sample was subsequently run on an SDS-PAGE gel, and slices were subsequently incubated in dithiothreitol (DTT), before being processed for LC-MS/MS (*22*). Using a protein database consisting of (1) predicted genes from the *M. capitata* nuclear genome assembly (version 3) (*50*); (2) predicted genes from the *Cladocopium goreaui* nuclear genome assembly (*52*) (3) predicted genes from the *Durusdinium trenchii* CCMP2556 nuclear genome assembly (*51*); (4) predicted genes from the *Montipora capitata* (OX421459.1) mitochondrial genome assembly; (5) predicted genes from the *Breviolum minutum* mitochondrial genome assembly (*53*); and (6) predicted genes from the *Cladocopium* C3 plastid genome assembly (*54*). The algal components of the database were chosen based on existing literature and through analysis of the available transcriptomic data from these samples. Precursor and fragment mass tolerances were set at ± 10 ppm and ± 0.5 Da (respectively) for the proteome. TMTpro and carbamiodomethyl on cysteine was set as static modifications. TMTpro was also set as the peptide N-terminus modification. Methionine oxidation was set as a dynamic modification; protein N-terminal acetylation, protein N-terminal methionine loss, and protein N-terminal methionine loss plus acetylation were set as dynamic modifications for protein termini.

Proteins without detectable abundance values in more than three samples were removed from downstream analysis. The two samples from different genotypes erroneously included at $TP5_H$ (MC-289_T5-Amb_1721 and MC-289_T5-HiT_2998) were removed from our analysis. We excluded $TP5_H$ from our analysis because both removed samples are from $TP5_H$ (one from high and one from ambient) and only two replicates per condition/time point are available for the proteomic data (leaving just one sample available for each of the conditions at $TP5_H$). No additional protein abundance adjustment (beyond the sample normalization performed by Proteome Discover) was performed on the data because, for the time points analyzed ($TP1_H$ and $TP3_H$), no significant shift in color score was observed (**Fig. S1B**).

GBR species data

Test species

A single large colony of *Acropora hyacinthus* (neat morphotype), *Stylophora pistillata*, and *Porites lobata* were sampled from Davies Reef (−18°49′30″S, 147°38′42″E) on the central GBR in February 2023 (Permit Number: G19:43148) (**Fig. 1B**). Only one genotype was used to avoid the possibility of stochastic inter-colony variation in the stress proteome and metabolome (*55*, *56*). These species were selected to represent different morphologies and heat stress sensitivities: *Acropora hyacinthus* - sensitive, tabulate, branching; *Stylophora pistillata* - sensitive, branching; *Porites lobata* - tolerant, massive.

Experimental design

Each colony was subdivided into 36 fragments (~7cm^2), mounted on experimental racks, and allowed to recover for 3 weeks prior to the start of the experiment at the National Sea Simulator (SeaSim) at the Australian Institute of Marine Science (AIMS) in outdoor flow through tanks replicating Davies Reef conditions (28.0°C, ca. ~250 µmol photons m^{-2} s^{-1}). Prior to heat stress treatments, fragments were randomly assigned across six indoor 50 L experimental flow through tanks (n = 18 per tank, 6 fragments per species), three for each of the two experimental treatments and acclimated for seven days before initiating heat stress. Fragments were exposed to two treatments: a temperature treatment of 32.4°C and a control maintained at 28.38^{o}C (Maximum Monthly Mean [MMM] at Davies Reef). The MMM is defined as the maximum sea surface temperature (SST) of the 12 monthly mean

values for the years 1985-1990 and 1993 (*57*). Temperature ramping increased from 28.38°C to 32.4°C, over 5 days (0.8°C/day) for treatment tanks. The heat stress experiment ran for a further 4 days concluding after 9 days. Heat exchangers and precision mixers were used to control tank water temperature within 0.1°C and programmed and monitored using the Supervisory Control and Data Acquisition system (SCADA) at SeaSim. Experimental tanks were immersed within temperature controlled exterior insulating jackets of seawater kept at treatment temperatures (one jacket per treatment) and each tank fitted with a TC Direct PT-100 temperature probe to maintain ramp rate and programmed temperatures. Filtered seawater was continuously supplied to the experimental system at an inflow rate of 0.8L/minute and each tank was fitted with a circulator (Turbelle nanostream 6015 3.5 W, Tunze Aquarientechnik Gmbh, Germany) for water movement. Light was on a 24 hour 12:12 light/dark cycle with a 2-hour sunrise/sunset ramp time (half-sine ramp) and maximum photosynthetically active radiation (PAR) at 280 µmol/m^2/s supplied from SS Gen 1 Customised multichip LEDs (325 W, The National Sea Simulator, Townsville, Australia) and measured continuously in each tank using a Li-192 sensor (UWQ8687, Li-COR, USA) and Li-250Am meter (Li-COR, USA). Water temperature and PAR was stable at target levels throughout the experiment.

Sampling plan

During the experiment, corals were sampled at three time points (**Fig. 1B**): TP_G denotes GBR samples. $TP0_G$ at the start of the experiment (end of coral acclimation described above) but prior to temperature ramping; $TP1_G$ on day 5 at the end of temperature ramping; and $TP2_G$, on day 9. At each timepoint, sampling included photographs of each fragment to assess health status and bleaching using the CoralWatch Health Chart (*58*) and one fragment per species from each tank (n = 3/treatment/species) was immediately snap frozen and kept at -80°C until processing for metabolomics, proteomics, and algal endosymbiont cell counts and typing (see below). At each timepoint, and additionally, on days 7 and 8, the maximal quantum yield (F_v/F_m) of chlorophyll a fluorescence of all fragments was measured using a Diving-PAM (Waltz, Germany; Fiberoptics outer diameter 8 mm; settings: measuring light intensity = 8, saturation pulse intensity = 11, saturating width = 0.8s, damping = 2, gain = 4). Measurements were made before dawn, therefore, colonies were low light acclimated (*59*). Each fragment was measured three times, and the average values were recorded.

The maximum treatment temperature (MMM) and ramp-up time were calibrated for each experiment (Hawai i and GBR) to ensure that the stress experienced by the corals was roughly equivalent in terms of expected response and ecological relevance. Light levels in the experimental set ups were set to 345 µmol/m^2/s and 280 µmol/m^2/s, respectively. The higher ramp-up rate utilized for the GBR experiment (0.8°C/day for 5 days) compared to the Hawaii ramp-up rate (0.4°C every two days, for 9 days) may have contributed to the divergent outcomes of the different species, however, based on the ecological and proteomic response, it was evident that corals in both experiments experienced roughly similar levels of stress.

GBR Endosymbiont physiology

Endosymbiont counts

A small section of tissue (~1 cm^2) from each frozen fragment collected at each timepoint ($TP0_G$, $TP1_G$, $TP2_G$), was air-brushed in PBS buffer, separated (as above), and washed three times in filtered seawater for endosymbiont cell counts. Cell quantification was

determined visually *via* a haemocytometer (Neubauer Haemocytometer, Fisher Scientific, Loughborough, UK) with eight replicate quadrats counted for each sample. We performed a two-tailed Welch t-test (n=3) for each timepoint and coral species.

Endosymbiont typing

A small section of tissue (~2 cm^2) from each frozen fragment collected at $TP0_G$ was air-brushed in PBS buffer to characterize Symbiodiniaceae communities based on amplicon sequencing of the ribosomal internal transcribed spacer 2 (ITS-2) region. The tissue slurry was centrifuged at 3000g for 10 minutes to separate the coral host and algal symbiont fractions. DNA was extracted from the algal pellet using the Qiagen DNeasy Blood and Tissue kit (Qiagen, Germany) following the "protocol: purification of total DNA from animal tissues" including a RNase A-based RNA digestion procedure. Genomic DNA was sent to the Ramaciotti Centre for Genomics (University of New South Wales, Sydney, Australia) and ITS-2 amplicons sequenced using the sym_var_5.8s2/sym_var_rev primers on the NextSeq 1000 P1 platform with 2x300bp paired-end sequencing (including PhiX spike-in) (*60*). ITS2 sequences were submitted to the SymPortal analytical framework for quality control and ITS2 type profile analysis (https://symportal.org) as described by Hume and coauthors (*61*).

Protein Extraction

Proteins were extracted using a RIPA lysis buffer, composed of Tris-HCl (50mM), NaCl (150mM), SDS (1%), and DI water. The buffer was chilled on ice until ready for use and one cOmplete mini EDTA-free tablet was dissolved in 10 ml of lysis buffer immediately before extraction. A total of 500µl of ice-cold RIPA lysis buffer was added to a tube filled with 0.5mm silica beads. Approximately 0.2-0.4 g of coral sample was clipped into each bead tube. The samples were vortexed for at least five minutes, or until the skeleton was stripped from the tissue. The samples were then incubated on ice for 30 minutes, before centrifuging at 10,000 rcf for 10 minutes and extracting the supernatant. Protein quality was assessed using a Qubit protein assay. Samples were stored at -80˚C freezer.

Proteomics analysis

Protein concentrations were assayed using the Qubit Protein Assay. Proteomic analysis was performed at the University of South Florida Proteomics Core. The proteins were normalized before digestion using 25µg for each sample. After digestion, an equal amount of sample (1000ng) was injected for each run. After digestion, an equal amount of sample (1000ng) was injected for each run. LC-MS analysis peptides were characterized using a Thermo Q-exactive-HF-X mass spectrometer coupled to a Thermo Easy nLC 1200. Samples separated at 300nl/min on an Acclaim PEPMAP 100 trap (75uM, 2CM, c18 3um, 100A) and an Thermo easy spray column (75um, 25cm, c18, 100A) using a 180-minute gradient with an initial starting condition of 2% B buffer (0.1% formic acid in 90% Acetonitrile) and 98% A buffer (0.1% formic acid in water). Buffer B was increased to 28% over 140 minutes, then up to 40% in an additional 10 minutes. High B (90%) was run for 15 minutes afterwards. The mass spectrometer was outfitted with a Thermo nanospray easy source with the following parameters: Spray voltage: 2.00V, Capillary temperature: 300dC, Funnel RF level=40. Parameters for data acquisition were as follows: for MS data the resolution was 60,000 with an AGC target of $3e^6$ and a max IT time of 50 ms, the range was set to 400-1600 m/z. MS/MS data was acquired with a resolution of 15,000, an AGC of $1e^4$, max IT of 50 ms, and the top 30 peaks were picked with an isolation window of 1.6m/z with a dynamic execution of 25s.

For each of the three species, a comprehensive metaproteomic database was assembled based on the ITS2 results (**Fig. S8**) to aid protein identification. A proteomic database for *Porites lobata* was assembled from: (1) predicted genes from the *P. lobata* transcriptome assembly (v1) (*62*); (2) predicted genes from the *P. lobata* (KU572435) mitochondrial genome assembly (*63*); (3) predicted genes from the *Cladocopium goreaui* nuclear genome assembly, (4) predicted genes from the *Breviolum minutum* mitochondrial genome assembly; and (5) predicted genes from the *Cladocopium* C3 plastid genome assembly. A proteomic database for *Acropora hyacinthus* was assembled from: (1) predicted genes from the *A. hyacinthus* nuclear genome assembly (v1) (*36*); (2) predicted genes from the *A. hyacinthus* (OP311657) mitochondrial genome assembly (*64*); (3) predicted genes from the *Cladocopium goreaui* nuclear genome assembly; (4) predicted genes from the *Breviolum minutum* mitochondrial genome assembly; and (5) predicted genes from the *Cladocopium* C3 plastid genome assembly. Finally, a proteomic database for *Stylophora pistillata* was assembled from: (1) predicted genes from the *S. pistillata* nuclear genome assembly (v1) (*65*); (2) predicted genes from the *S. pistillata* (EU400214) mitochondrial genome assembly; (3) predicted genes from the *Cladocopium goreaui* nuclear genome assembly; (4) predicted genes from the *Breviolum minutum* mitochondrial genome assembly; and (5) predicted genes from the *Cladocopium* C3 plastid genome assembly.

Samples were processed using Max quant 2.0.3.1. The metaproteomic databases described above for each species were searched with the following parameters: tryptic enzyme with a max of 2 missed cleavages, a precursor mass tolerance of 10ppm and a fragment mass tolerance of 0.02 Da. Modifications included Oxidation, Acetyl, and Carbamidomethyl. The FDR rate was set at 0.01, label free quantification (LFQ) intensities were compared between samples for ID. The Perseus analysis software was used to sort and filter data, features being retained if they were identified in at least 66% of samples in each group. Note that only log and non-log data were calculated. Proteins without detectable abundance values in more than three samples were removed. Due to the clear decrease in endosymbiont cell density at $TP2_G$, endosymbiont proteins from the GBR, identified in the proteome data had their intensity values adjusted based on the observed change in their cell counts over the course of the experiment. For each time point (n = 3), the ratio between the $\log_2$ symbiont cell density values of the ambient and high temperate samples were calculated, and the resulting ratios were multiplied against the corresponding high temperate samples (e.g., the $\log_2$ ratio between $TP2_G$ ambient and high temperate samples was multiplied against the $TP2_G$ high temperature sample symbiont protein intensity values). This symbiont cell density adjustment was done to account for cell loss during thermal stress, thereby reducing any variation in protein abundance due to bleaching. These cell-abundance adjusted values were subsequently used for all downstream endosymbiont protein abundance analysis.

Metabolomic analysis

In addition to the physiological measurements and metaproteomics work described below for the Hawaiian and GBR research, we also generated untargeted polar metabolomics data from the GBR corals used for the thermal stress experiment. Our goal was to assess the abundance of metabolites (most notably, dipeptides such as arginine-glutamine), whose increasing abundance has previously been shown to be associated with the thermal stress response in *M. capitata* and other Hawaiian coral species (*37*). Metabolites were extracted using a protocol optimized for water-soluble polar metabolite analysis on LC-MS. The extraction buffer was a solution of 40:40:20 (methanol:acetonitrile:water) (v/v/v)

+ 0.1 M formic acid. The extraction buffer was stored at −20°C before usage. Immediately preceding the metabolite extraction, 1 ml of extraction buffer was added to the 2ml tube with glass beads. Pieces (~0.2-0.4 g) of the -80°C preserved nubbins were then clipped, weighed, and added. The coral samples were then homogenized. The rest of the homogenate was then transferred to a 1.5-ml Eppendorf tube, vortexed for 10 s, and then centrifuged for 10 min at 14,000*g* at 4°C. After centrifugation, there was a pellet at the bottom of the tube. A final 500-µl aliquot of the homogenate was then pipetted to a second clean Eppendorf tube, to which 44 µl of 15% NH_4HCO_3 was added to neutralize the acid in the buffer. This was the final extract and was transferred to autosampler vials to be loaded to instrument.

Prior to running the samples, the LC-MS system was evaluated for performance readiness by running a commercially available standard mixture and an in-house standard mixture to assess the mass accuracy, signal intensities and the retention time consistency. All known metabolites in the mixture were detected to within 5ppm mass accuracy. Method blank samples matching the composition of the extraction solvent were used in every sample batch to assess background signals and ensure there was no carryover from one run to the next. In addition, the sample queue was randomized with respect to sample treatment to eliminate the potential for batch effects.

The HILIC separation was performed on a Vanquish Horizon UHPLC system (Thermo Fisher Scientific, Waltham, MA) with XBridge BEH Amide column (150 mm × 2.1 mm, 2.5 µm particle size, Waters, Milford, MA) using a gradient of solvent A (95%:5% H 2 O:acetonitrile with 20 mM acetic acid, 40 mM ammonium hydroxide, pH 9.4), and solvent B (20%:80% H 2 O:acetonitrile with 20 mM acetic acid, 40 mM ammonium hydroxide, pH 9.4). The gradient was 0 min, 100% B; 3 min, 100% B; 3.2 min, 90% B; 6.2 min, 90% B; 6.5 min, 80% B; 10.5 min, 80% B; 10.7 min, 70% B; 13.5 min, 70% B; 13.7 min, 45% B; 16 min, 45% B; 16.5 min, 100% B and 22 min, 100% B (*66*) . The flow rate was 300 µl/min. Injection volume was 5 µL and column temperature was 25 °C. The autosampler temperature was set to 4°C and the injection volume was 5µL.

The full scan mass spectrometry analysis was performed on a Thermo Q Exactive PLUS with a HESI source which was set to a spray voltage of -2.7kV under negative mode and 3.5kV under positive mode. The sheath, auxiliary, and sweep gas flow rates of 40, 10, and 2 (arbitrary unit) respectively. The capillary temperature was set to 300 °C and aux gas heater was 360 °C. The S-lens RF level was 45. The m/z scan range was set to 72 to 1000 m/z under both positive and negative ionization mode. The AGC target was set to 3e6 and the maximum IT was 200ms. The resolution was set to 70,000.

The full scan data were processed with a targeted data pipeline using MAVEN software package (*67*). Compound identification was assessed using accurate mass and retention time match to the metabolite standards from the in-house library. Metabolites in the targeted dataset were filtered for low abundance: i.e., if more than 3 replicates had no detected intensity, they were excluded from downstream analysis.

We subsequently calculated the $\log_2$FC for each of the metabolites across the species, using Python (v.3.9.12) (additional packages pandas v1.4.2 and numpy v1.26.4), comparing the ambient and the stressed corals at each timepoint. We also assessed the statistical significance for each of the metabolites using a Welch t-test (n = 3 for Hawai i

experiments and n=6 for GBR experiments) with multiple testing correction using the Benjamini-Hochberg procedure, using SciPy (v1.12.0).

Combined metaproteomic data analysis

For downstream analysis, we utilized label free quantification (LFQ) values from the Perseus computational platform for all three GBR coral species. Proteins identified in the proteomic data were separated by origin (i.e., algal or coral) before analysis. GhostKOALA (v2.0) (*68*); was used to annotate proteins with KEGG Orthology (KO) numbers. Furthermore, eggNOG-mapper (v2.1.6; database release 2021-12-09) (*69*) was used to annotate host proteins, supplementing the KEGG annotations with functions not part of existing KEGG pathways. We subsequently calculated the $\log_2$FC for each of the using Python (v.3.9.12) (additional packages pandas v1.4.2 and numpy v1.26.4), and SciPy (v1.12.0) to assess statistical significance using a Welch t-test (n=3) of proteins between the ambient and high temperature samples from $TP1_H$ and $TP3_H$ (for *M. capitata)* and for $TP0_G$, $TP1_G$, and $TP2_G$ (for the three GBR coral species). The two datasets were integrated by comparing the results from *M. capitata* $TP1_H$ and GBR corals $TP1_G$ together, and the results from *M. capitata* $TP3_H$ and GBR corals $TP2_G$ together.

The total proteome (i.e., host and endosymbiont) was uploaded to KEGG Mapper to provide an overview of protein coverage within each pathway (*70*, *71*). The stress response proteome (i.e., all host and endosymbiont proteins that showed differential accumulation with an absolute FC > 0.5 between ambient and treatment conditions at any timepoint) was uploaded in a separate analysis. The KEGG pathways identified in the stress response proteome with at least one protein with a *p*-value < 0.05 (i.e., significant *p*-value) and two differentially accumulated proteins were selected for further analysis. The functions of endosymbiont and host proteins in the stress response proteome identified by KEGG Mapper as being part of key pathways were verified using BLASTp (v.2.13.0) against the NCBI nr database. Last, we also performed a principal component analysis (PCA) utilizing Base R (v4.2.1) to assess proteome distribution in coral hosts and endosymbionts.

References

1. B. R. Gordon, W. Leggat, Symbiodinium—Invertebrate Symbioses and the Role of Metabolomics. *Marine Drugs* **8**, 2546–2568 (2010).

2. K. Frankowiak, X. T. Wang, D. M. Sigman, A. M. Gothmann, M. V. Kitahara, M. Mazur, A. Meibom, J. Stolarski, Photosymbiosis and the expansion of shallow-water corals. *Science Advances* **2**, e1601122 (2016).

3. L. Muscatine, J. W. Porter, Reef Corals: Mutualistic Symbioses Adapted to Nutrient-Poor Environments. *BioScience* **27**, 454–460 (1977).

4. A. G. Grottoli, L. J. Rodrigues, J. E. Palardy, Heterotrophic plasticity and resilience in bleached corals. *Nature* **440**, 1186–1189 (2006).

5. Y. Loya, K. Sakai, K. Yamazato, Y. Nakano, H. Sambali, R. van Woesik, Coral bleaching: the winners and the losers. *Ecology Letters* **4**, 122–131 (2001).

6. K. L. Barott, A. A. Venn, S. O. Perez, S. Tambutté, M. Tresguerres, Coral host cells acidify symbiotic algal microenvironment to promote photosynthesis. *Proceedings of the National Academy of Sciences of the United States of America* **112**, 607–612 (2015).

7. K. L. Barott, A. B. Thies, M. Tresguerres, V-type H^+-ATPase in the symbiosome membrane is a conserved mechanism for host control of photosynthesis in anthozoan photosymbioses. *Royal Society Open Science* **9**, 211449 (2022).

8. S. Martinez, R. Grover, C. Ferrier-Pagès, Symbiont starvation affects the stability of the coral–Symbiodiniaceae symbiosis. *Frontiers in Marine Science* **9**, 979563 (2022).

9. N. Rädecker, C. Pogoreutz, H. M. Gegner, A. Cárdenas, F. Roth, J. Bougoure, P. Guagliardo, C. Wild, M. Pernice, J.-B. Raina, A. Meibom, C. R. Voolstra, Heat stress destabilizes symbiotic nutrient cycling in corals. *Proceedings of the National Academy of Sciences of the United States of America* **118**, e2022653118 (2021).

10. K. Maor-Landaw, M. Eisenhut, G. Tortorelli, A. van de Meene, S. Kurz, G. Segal, M. J. H. van Oppen, A. P. M. Weber, G. I. McFadden, A candidate transporter allowing symbiotic dinoflagellates to feed their coral hosts. *ISME Communications* **3**, 7 (2023).

11. A. B. Thies, A. R. Quijada-Rodriguez, H. Zhouyao, D. Weihrauch, M. Tresguerres, A Rhesus channel in the coral symbiosome membrane suggests a novel mechanism to regulate NH3 and CO2 delivery to algal symbionts. *Science Advances* **8**, eabm0303.

12. E. R. Graham, A. Parekh, R. K. Devassy, R. W. Sanders, Carbonic anhydrase activity changes in response to increased temperature and pCO2 in *Symbiodinium*–zoanthid associations. *Journal of Experimental Marine Biology and Ecology* **473**, 218–226 (2015).

13. D. Zoccola, P. Ganot, A. Bertucci, N. Caminiti-Segonds, N. Techer, C. R. Voolstra, M. Aranda, E. Tambutté, D. Allemand, J. R. Casey, S. Tambutté, Bicarbonate transporters in corals point towards a key step in the evolution of cnidarian calcification. *Scientific Reports* **5**, 9983 (2015).

14. S. Martinez, Y. Kolodny, E. Shemesh, F. Scucchia, R. Nevo, S. Levin-Zaidman, Y. Paltiel, N. Keren, D. Tchernov, T. Mass, Energy Sources of the Depth-Generalist Mixotrophic Coral *Stylophora pistillata*. *Frontiers of Marine Science* **7**, 566663 (2020).

15. S. Martinez, R. Grover, D. M. Baker, C. Ferrier-Pagès, Symbiodiniaceae Are the First Site of Heterotrophic Nitrogen Assimilation in Reef-Building Corals. *mBio* **13**, e01601-22 (2022).

16. C. Downs, J. Fauth, J. Halas, P. Dustan, J. Bemiss, C. Woodley, Oxidative stress and seasonal coral bleaching. *Free Radical Biology & Medicine* **33**, 533–43 (2002).

17. M. P. Lesser, Oxidative stress causes coral bleaching during exposure to elevated temperatures. *Coral Reefs* **16**, 187–192 (1997).

18. N. Rosic, J. Delamare-Deboutteville, S. Dove, Heat stress in symbiotic dinoflagellates: Implications on oxidative stress and cellular changes. *Science of The Total Environment* **944**, 173916 (2024).

19. S. R. Dunn, M. Pernice, K. Green, O. Hoegh-Guldberg, S. G. Dove, Thermal stress promotes host mitochondrial degradation in symbiotic cnidarians: are the batteries of the reef going to run out? *PLOS ONE* **7**, e39024 (2012).

20. D. Tolleter, F. O. Seneca, J. C. DeNofrio, C. J. Krediet, S. R. Palumbi, J. R. Pringle, A. R. Grossman, Coral Bleaching Independent of Photosynthetic Activity. *Current Biology* **23**, 1782–1786 (2013).

21. L. J. Cowen, H. M. Putnam, Bioinformatics of Corals: Investigating Heterogeneous Omics Data from Coral Holobionts for Insight into Reef Health and Resilience. *Annual Review of Biomedical Data Science* **5**, 205–231 (2022).

22. A. Williams, T. G. Stephens, A. Shumaker, D. Bhattacharya, Peeling back the layers of coral holobiont multi-omics data. *iScience* **26**, 107623 (2023).

23. A. Ghazalpour, B. Bennett, V. A. Petyuk, L. Orozco, R. Hagopian, I. N. Mungrue, C. R. Farber, J. Sinsheimer, H. M. Kang, N. Furlotte, C. C. Park, P.-Z. Wen, H. Brewer, K. Weitz, D. G. Camp, C. Pan, R. Yordanova, I. Neuhaus, C. Tilford, N. Siemers, P. Gargalovic, E. Eskin, T. Kirchgessner, D. J. Smith, R. D. Smith, A. J. Lusis, Comparative Analysis of Proteome and Transcriptome Variation in Mouse. *PLoS Genetics* **7**, e1001393 (2011).

24. S. P. Gygi, Y. Rochon, B. R. Franza, R. Aebersold, Correlation between protein and mRNA abundance in yeast. *Molecular and Cellular Biology* **19**, 1720–1730 (1999).

25. T. Maier, M. Güell, L. Serrano, Correlation of mRNA and protein in complex biological samples. *FEBS Letters* **583**, 3966–3973 (2009).

26. C. Buccitelli, M. Selbach, mRNAs, proteins and the emerging principles of gene expression control. *Nature Reviews Genetics* **21**, 630–644 (2020).

27. L. Tomanek, Proteomics to study adaptations in marine organisms to environmental stress. *Journal of Proteomics* **105**, 92–106 (2014).

28. L. Tomanek, Environmental proteomics: changes in the proteome of marine organisms in response to environmental stress, pollutants, infection, symbiosis, and development. *Annual Review of Marine Science* **3**, 373–399 (2011).

29. S. Thangaraj, S. K. Palanisamy, G. Zhang, J. Sun, Quantitative proteomic profiling of marine diatom *Skeletonema dohrnii* in response to temperature and silicate induced environmental stress. *Frontiers in Microbiology* **11**, 554832 (2021).

30. M. Fan, X. Sun, Z. Liao, J. Wang, Y. Li, N. Xu, Comparative proteomic analysis of *Ulva prolifera* response to high temperature stress. *Proteome Science* **16**, 17 (2018).

31. L. Tomanek, M. J. Zuzow, The proteomic response of the mussel congeners *Mytilus galloprovincialis* and *M. trossulus* to acute heat stress: implications for thermal tolerance limits and metabolic costs of thermal stress. *Journal of Experimental Biology* **213**, 3559–3574 (2010).

32. M. Stuhr, B. Blank-Landeshammer, C. E. Reymond, L. Kollipara, A. Sickmann, M. Kucera, H. Westphal, Disentangling thermal stress responses in a reef-calcifier and its photosymbionts by shotgun proteomics. *Scientific Reports* **8**, 3524 (2018).

33. K. Petrou, B. L. Nunn, M. P. Padula, D. J. Miller, D. A. Nielsen, Broad scale proteomic analysis of heat-destabilised symbiosis in the hard coral *Acropora millepora*. *Scientific Reports* **11**, 19061 (2021).

34. M. E. Warner, W. K. Fitt, G. W. Schmidt, Damage to photosystem II in symbiotic dinoflagellates: A determinant of coral bleaching. *Proceedings of the National Academy of Sciences of the United States of America* **96**, 8007–8012 (1999).

35. W. K. Fitt, R. D. Gates, O. Hoegh-Guldberg, J. C. Bythell, A. Jatkar, A. G. Grottoli, M. Gomez, P. Fisher, T. C. Lajuenesse, O. Pantos, R. Iglesias-Prieto, D. J. Franklin, L. J. Rodrigues, J. M. Torregiani, R. van Woesik, M. P. Lesser, Response of two species of Indo-Pacific corals, *Porites cylindrica* and *Stylophora pistillata*, to short-term thermal stress: The host does matter in determining the tolerance of corals to bleaching. *Journal of Experimental Marine Biology and Ecology* **373**, 102–110 (2009).

36. T. Singh, M. Iijima, K. Yasumoto, K. Sakai, Effects of moderate thermal anomalies on *Acropora* corals around Sesoko Island, Okinawa. *PLoS ONE* **14**, e0210795 (2019).

37. A. Williams, E. N. Chiles, D. Conetta, J. S. Pathmanathan, P. A. Cleves, H. M. Putnam, X. Su, D. Bhattacharya, Metabolomic shifts associated with heat stress in coral holobionts. *Science Advances* **7**, eabd4210 (2021).

38. A. Williams, J. S. Pathmanathan, T. G. Stephens, X. Su, E. N. Chiles, D. Conetta, H. M. Putnam, D. Bhattacharya, Multi-omic characterization of the thermal stress phenome in the stony coral *Montipora capitata*. *PeerJ* **9**, e12335 (2021).

39. M. Stat, X. Pochon, E. C. Franklin, J. F. Bruno, K. S. Casey, E. R. Selig, R. D. Gates, The distribution of the thermally tolerant symbiont lineage (*Symbiodinium* clade D) in corals from Hawaii: correlations with host and the history of ocean thermal stress. *Ecology and Evolution* **3**, 1317–1329 (2013).

40. M. Stat, C. E. Bird, X. Pochon, L. Chasqui, L. J. Chauka, G. T. Concepcion, D. Logan, M. Takabayashi, R. J. Toonen, R. D. Gates, Variation in *Symbiodinium* ITS2 sequence assemblages among coral colonies. *PLoS One* **6**, e15854 (2011).

41. J. B. Axworthy, E. Timmins-Schiffman, T. Brown, L. J. Rodrigues, B. L. Nunn, J. L. Padilla-Gamiño, Shotgun Proteomics Identifies Active Metabolic Pathways in Bleached Coral Tissue and Intraskeletal Compartments. *Frontiers in Marine Science* **9** (2022).

42. E. N. Chiles, A. S. Huffmyer, C. Drury, H. M. Putnam, D. Bhattacharya, X. Su, Stable isotope tracing reveals compartmentalized nitrogen assimilation in scleractinian corals. *Frontiers in Marine Science* **9**, 1035523 (2022).

43. Luke A. Morris, Christian R. Voolstra, Kate M. Quigley, David G. Bourne, Line K. Bay, Nutrient availability and metabolism affect the stability of coral–Symbiodiniaceae symbioses, *Trends in Microbiology*, **8,** 678-689 (2019).

44. M. Schweinsberg, F. Gösser, R. Tollrian, The history, biological relevance, and potential applications for polyp bailout in corals. *Ecology and Evolution* **11**, 8424–8440 (2021).

45. R. H. McLachlan, J. T. Price, A. Muñoz-Garcia, N. L. Weisleder, S. J. Levas, C. P. Jury, R. J. Toonen, A. G. Grottoli, Physiological acclimatization in Hawaiian corals following a 22-month shift in baseline seawater temperature and pH. *Scientific Reports* **12**, 3712 (2022).

46. A. M. Bolger, M(*1*). Lohse, B. Usadel, Trimmomatic: a flexible trimmer for Illumina sequence data. *Bioinformatics* **30**, 2114–2120 (2014).

47. A. Shumaker, H. M. Putnam, H. Qiu, D. C. Price, E. Zelzion, A. Harel, N. E. Wagner, R. D. Gates, H. S. Yoon, D. Bhattacharya, Genome analysis of the rice coral *Montipora capitata*. *Scientific Reports* **9**, 2571 (2019).

48. D. Kim, J. M. Paggi, C. Park, C. Bennett, S. L. Salzberg, Graph-based genome alignment and genotyping with HISAT2 and HISAT-genotype. *Nature Biotechnology* **37**, 907–915 (2019).

49. M. G. Grabherr, B. J. Haas, M. Yassour, J. Z. Levin, D. A. Thompson, I. Amit, X. Adiconis, L. Fan, R. Raychowdhury, Q. Zeng, Z. Chen, E. Mauceli, N. Hacohen, A. Gnirke, N. Rhind, F. di Palma, B. W. Birren, C. Nusbaum, K. Lindblad-Toh, N. Friedman, A. Regev, Full-length transcriptome assembly from RNA-Seq data without a reference genome. *Nature Biotechnology* **29**, 644–652 (2011).

50. T. G. Stephens, J. Lee, Y. Jeong, H. S. Yoon, H. M. Putnam, E. Majerová, D. Bhattacharya, High-quality genome assemblies from key Hawaiian coral species. *GigaScience* **11**, giac098 (2022).

51. K. E. Dougan, A. J. Bellantuono, T. Kahlke, R. M. Abbriano, Y. Chen, S. Shah, C. Granados-Cifuentes, M. J. H. van Oppen, D. Bhattacharya, D. J. Suggett, M. Rodriguez-Lanetty, C. X. Chan, Whole-genome duplication in an algal symbiont bolsters coral heat tolerance. *Science Advances* **10**, eadn2218 (2024).

52. Y. Chen, S. Shah, K. E. Dougan, M. J. H. van Oppen, D. Bhattacharya, C. X. Chan, Improved *Cladocopium goreaui* Genome Assembly Reveals Features of a Facultative Coral Symbiont and the Complex Evolutionary History of Dinoflagellate Genes. *Microorganisms* **10**, 1662 (2022).

53. E. Shoguchi, C. Shinzato, K. Hisata, N. Satoh, S. Mungpakdee, The Large Mitochondrial Genome of *Symbiodinium minutum* Reveals Conserved Noncoding Sequences between Dinoflagellates and Apicomplexans. *Genome Biology and Evolution* **7**, 2237–2244 (2015).

54. A. C. Barbrook, C. R. Voolstra, C. J. Howe, The Chloroplast Genome of a *Symbiodinium* sp. Clade C3 Isolate. *Protist* **165**, 1–13 (2014).

55. E. R. Andersson, R. D. Day, J. M. Loewenstein, C. M. Woodley, T. B. Schock, Evaluation of Sample Preparation Methods for the Analysis of Reef-Building Corals Using 1H-NMR-Based Metabolomics. *Metabolites* **9**, 32 (2019).

56. M. Sweet, M. Bulling, D. Varshavi, G. R. Lloyd, A. Jankevics, L. Najdekr, R. J. M. Weber, M. R. Viant, J. Craggs, Species-Specific Variations in the Metabolomic Profiles of *Acropora hyacinthus* and *Acropora millepora* Mask Acute Temperature Stress Effects in Adult Coral Colonies. *Frontiers in Marine Science* **8** (2021).

57. S. F. Heron, G. Liu, C. M. (Carlon M. Eakin, W. J. (William J. Skirving, F. E. Muller-Karger, M. Vega-Rodriguez, J. L. De La Cour, T. F. R. Burgess, A. E. (Alan E. Strong, E. F. Geiger, L. S. Guild, S. Lynds, Climatology development for NOAA Coral Reef Watch's 5-km product suite. doi: 10.7289/V59C6VBS (2014).

58. U. E. Siebeck, N. J. Marshall, A. Klüter, O. Hoegh-Guldberg, Monitoring coral bleaching using a colour reference card. *Coral Reefs* **25**, 453–460 (2006).

59. D. J. Suggett, M. R. Nitschke, D. J. Hughes, N. Bartels, E. F. Camp, N. Dilernia, J. Edmondson, S. Fitzgerald, A. Grima, A. Sage, M. E. Warner, Toward bio□optical phenotyping of reef□forming corals using Light□Induced FluorescenceTransient□FastRepetition Rate fluorometry. *Limnology and Oceanography: Methods* **20**, 172–191 (2022).

60. B. C. C. Hume, M. Ziegler, J. Poulain, X. Pochon, S. Romac, E. Boissin, C. de Vargas, S. Planes, P. Wincker, C. R. Voolstra, An improved primer set and amplification protocol with increased specificity and sensitivity targeting the *Symbiodinium* ITS2 region. *PeerJ* **6**, e4816 (2018).

61. B. C. C. Hume, E. G. Smith, M. Ziegler, H. J. M. Warrington, J. A. Burt, T. C. LaJeunesse, J. Wiedenmann, C. R. Voolstra, SymPortal: A novel analytical framework and platform for coral algal symbiont next-generation sequencing ITS2 profiling. *Molecular Ecology Resources* **19**, 1063–1080 (2019).

62. D. Bhattacharya, S. Agrawal, M. Aranda, S. Baumgarten, M. Belcaid, J. L. Drake, D. Erwin, S. Foret, R. D. Gates, D. F. Gruber, B. Kamel, M. P. Lesser, O. Levy, Y. J. Liew, M. MacManes, T. Mass, M. Medina, S. Mehr, E. Meyer, D. C. Price, H. M. Putnam, H. Qiu, C. Shinzato, E. Shoguchi, A. J. Stokes, S. Tambutté, D. Tchernov, C. R. Voolstra, N. Wagner, C. W. Walker, A. P. Weber, V. Weis, E. Zelzion, D. Zoccola, P. G. Falkowski, Comparative genomics explains the evolutionary success of reef-forming corals. *eLife* **5**, e13288 (2016).

63. K. H. Tisthammer, Z. H. Forsman, V. L. Sindorf, T. L. Massey, C. R. Bielecki, R. J. Toonen, The complete mitochondrial genome of the lobe coral *Porites lobata* (Anthozoa: Scleractinia) sequenced using ezRAD. *Mitochondrial DNA Part B* **1**, 247–249 (2016).

64. W. Wang, B. Cao, Z. Xu, Z. Jia, S. Yu, P. Tian, W. Niu, J. Xiao, The complete mitochondrial genome of *Montipora vietnamensis* (Scleractinia, Acroporidae). *Biodiversity Data Journal* **10**, e91531 (2022).

65. C. R. Voolstra, Y. Li, Y. J. Liew, S. Baumgarten, D. Zoccola, J.-F. Flot, S. Tambutté, D. Allemand, M. Aranda, Comparative analysis of the genomes of *Stylophora pistillata* and *Acropora digitifera* provides evidence for extensive differences between species of corals. *Scientific Reports* **7**, 17583 (2017).

66. X. Su, E. Chiles, S. Maimouni, F. E. Wondisford, W.-X. Zong, C. Song, In-Source CID Ramping and Covariant Ion Analysis of Hydrophilic Interaction Chromatography Metabolomics. *Analytical Chemistry* **92**, 4829–4837 (2020).

67. E. Melamud, L. Vastag, J. D. Rabinowitz, Metabolomic Analysis and Visualization Engine for LC−MS Data. *Analytical Chemistry* **82**, 9818–9826 (2010).

68. M. Kanehisa, Y. Sato, K. Morishima, BlastKOALA and GhostKOALA: KEGG Tools for Functional Characterization of Genome and Metagenome Sequences. *Journal of Molecular Biology* **428**, 726–731 (2016).

69. C. P. Cantalapiedra, A. Hernández-Plaza, I. Letunic, P. Bork, J. Huerta-Cepas, eggNOG-mapper v2: Functional Annotation, Orthology Assignments, and Domain Prediction at the Metagenomic Scale. *Molecular Biology and Evolution* **38**, 5825–5829 (2021).

70. M. Kanehisa, Y. Sato, KEGG Mapper for inferring cellular functions from protein sequences. *Protein Science* **29**, 28–35 (2020).

71. M. Kanehisa, Y. Sato, M. Kawashima, KEGG mapping tools for uncovering hidden features in biological data. *Protein Science* **31**, 47–53 (2022).

72. E. C. Franklin, P. L. Jokiel, M. J. Donahue. Predictive modeling of coral distribution and abundance in the Hawaiian Islands. *Marine Ecology Progress Series* **481**, 121-132 (2013).

73. E. C. Franklin, P. L. Jokiel, M. J. Donahue. Data from: Predictive modeling of coral distribution and abundance in the Hawaiian Islands. Dryad Digital Repository. https://doi.org/10.5061/dryad.9vd0q (2014).

Acknowledgments

We acknowledge the Bindal and Wulgurukaba Peoples as the Traditional Custodians of the land and sea Countries where the Great Barrier Reef part of this research took place. We wish to acknowledge Elders past, present, and emerging, and their continuing spiritual connection to sea Country. Thank you to the staff of the AIMS vessel and the National Sea Simulator for field and laboratory support. We also thank Elizabeth Wood at the University of South Florida, Proteomics Core for support with proteomic data collection and analysis. We thank Eric Chiles and Dr. Xiaoyang Su at the Rutgers Metabolomic Core. Finally, we wish to thank Eric Hochberg from the Bermuda Institute of Ocean Sciences for his contributions to the design of the study and assistance with collection of the samples.

Funding:

National Science Foundation award titled “Collaborative Research: Edge CMT: Polygenic traits of heat stress phenome in coral "dark genes" from genome to functional applications” (#2128073; 12/01/2021 to 11/30/2025) awarded to DB, USDA National Institute of Food and Agriculture Hatch Formula award titled “Using multi-omics and experimental evolution to understand the response of eukaryotes to changing environmental conditions” (#NJ01180; 01/17/20 to 09/30/24) awarded to DB, Revive & Restore award titled “Toward predictive coral phenomics” (#2022-039; 01/10/2022 to 09/30/2025) awarded to LKB, SG, and DB, and the Australian Government Reef Trust and Great Barrier Reef Foundation titled “Reef Restoration and Adaptation Program (RRAP)” awarded to SG and LKB.

Author contributions:

Shrinivas Nandi: Writing - original draft, Conceptualization, Investigation, Writing – review & editing, Methodology, Resources, Data curation, Validation, Formal analysis, Software, Visualization.
Timothy G. Stephens: Writing - original draft, Conceptualization, Writing – review & editing, Methodology, Validation.
Erin E. Chille: Writing- original draft, Conceptualization, Investigation, Writing – review & editing, Methodology, Validation.

Samantha Goyen: Investigation, Writing – review & editing, Methodology, Resources, Funding acquisition, Data curation, Validation, Formal analysis, Visualization.
Line K. Bay: Conceptualization, Investigation, Writing – review & editing, Methodology, Resources, Funding acquisition, Supervision, Project administration.
Debashish Bhattacharya: Writing - original draft, Conceptualization, Writing – review & editing, Methodology, Resources, Funding acquisition, Validation, Supervision, Project administration, Visualization.

Competing interests: Authors declare that they have no competing interests.

Data and materials availability: All data are available in the main text or the supplementary materials. The GBR coral mass spectrometry proteomics data have been deposited to the ProteomeXchange Consortium *via* the PRIDE partner repository with the dataset identifier PXD052478 (https://www.ebi.ac.uk/pride/). The metabolomic mass spectrometry data are available from the MassIVE database with the dataset identifier MSV000094832 (https://massive.ucsd.edu/). The ITS2 sequence read files are available from the Sequencing Read Archive (SRA) with the dataset identifier PRJNA1119670 (https://www.ncbi.nlm.nih.gov/sra/).

Figures and Tables

Fig. 1. Study sites and experimental designs. (**A**) Kāneʻohe Bay, Oʻahu, Hawai□i where the studied *M. capitata* was collected (n=14). The scaled percent cover of this species in the bay is shown. Image adapted from the Pacific Islands Ocean Observing System (*72*, *73*). The red thermometer represents the treatment tanks. TP_H refers to timepoints from the Hawai□i experiment. The experimental design for the *M. capitata* thermal stress work is shown in the right panel. (**B**) The location of collection and experimental design (right panel) for the GBR work are shown (n=48). Coral images from Samantha Goyen, map created in R using the Environmental Systems Research Institute (ESRI) shapefiles and Mapdata package, experimental setup image made in Canva. TP_G refers to timepoints from the GBR experiment.

Fig. 2. Dipeptide accumulation patterns in the three GBR corals. For each treatment (n = 6; blue for ambient samples and yellow for heat treated samples) at each time point (x-axis) the abundance (ion intensity) of each dipeptide is shown using a box plots. With the box representing the interquartile range, the whiskers represent the range of data outside the first quartile and third quartile within 1.5 times the interquartile range, and each sample shown as a colored point. Each row represents a different dipeptide analyzed in the study, and the columns are the respective coral species used in the study. *Represents significant metabolites (p-value < 0.05).

Fig. 3: Results of metaproteomic analysis of corals. (**A**) Stacked bar chart showing the number of proteins with a |FC| > 0.5 in the endosymbiont proteome from pathways of interest. Bars below zero on the y-axis indicate proteins with decreased abundance and bars above zero on the y-axis indicate proteins with increased abundance. The colored segments in each bar show the number of proteins with a given direction of accumulation from a given metabolic pathway. The numbers on the bar plots represent the number of proteins that were differentially accumulated and were also statistically significant (p-value < 0.05). The numerical data for the plot are available in **Table S10**. (**B**) Stacked bar chart showing the number of proteins with a |FC| > 0.5 in the host proteome from pathways of interest. The numerical data for the plot are available in **Tables S9, S10, and S11**. A legend describing the colors is shown in the top right of the figure.

Fig. 4. Proposed progression from ambient symbiosis to dysbiosis in *M. capitata* during thermal stress. Our proposed model for coral-algal dysbiosis, starting at an (**A**) ambient non-stressed state, and progressing from (**B**) initial to the (**C**) late stress response. Initial thermal stress ($TP1_H$) refers to the day temperature ramping was complete (9 days of temperature ramping). Late thermal stress ($TP3_H$) was 13 days after temperature ramping was complete. The thick blue arrows indicate lowered protein abundance, the thick red arrows indicate elevated protein abundance, and the black arrows indicate no change in the regulation of a pathway/enzyme.

Fig. 5. Divergent outcomes of thermal stress triggered endosymbiont dampening in three GBR coral species. (**A**) Diagram depicting a healthy symbiosis between the host and algal endosymbiont, involving transfer of nutrients from the host to the endosymbiont and subsequent transfer of photosynthates from the endosymbiont to the host. (**B**) Metabolic effects of endosymbiont dampening upon exposure to thermal stress. (**C**) The divergent host metabolic responses of the three studied GBR coral species. In each panel, blue arrows represent pathways with proteins that decrease in abundance in response to thermal

stress. A blue cross represents the lack of transfer of photosynthates from the endosymbiont to the host. The color of the endosymbiont provides graphical context of the endosymbiont dampening, that is, red represents higher metabolic activity of the endosymbiont, whereas shades of yellow represent lower endosymbiont metabolic activity. A combination of blue and red arrows represents a mixed protein response: i.e., a similar number of proteins in a pathway had increasing and decreasing abundances.

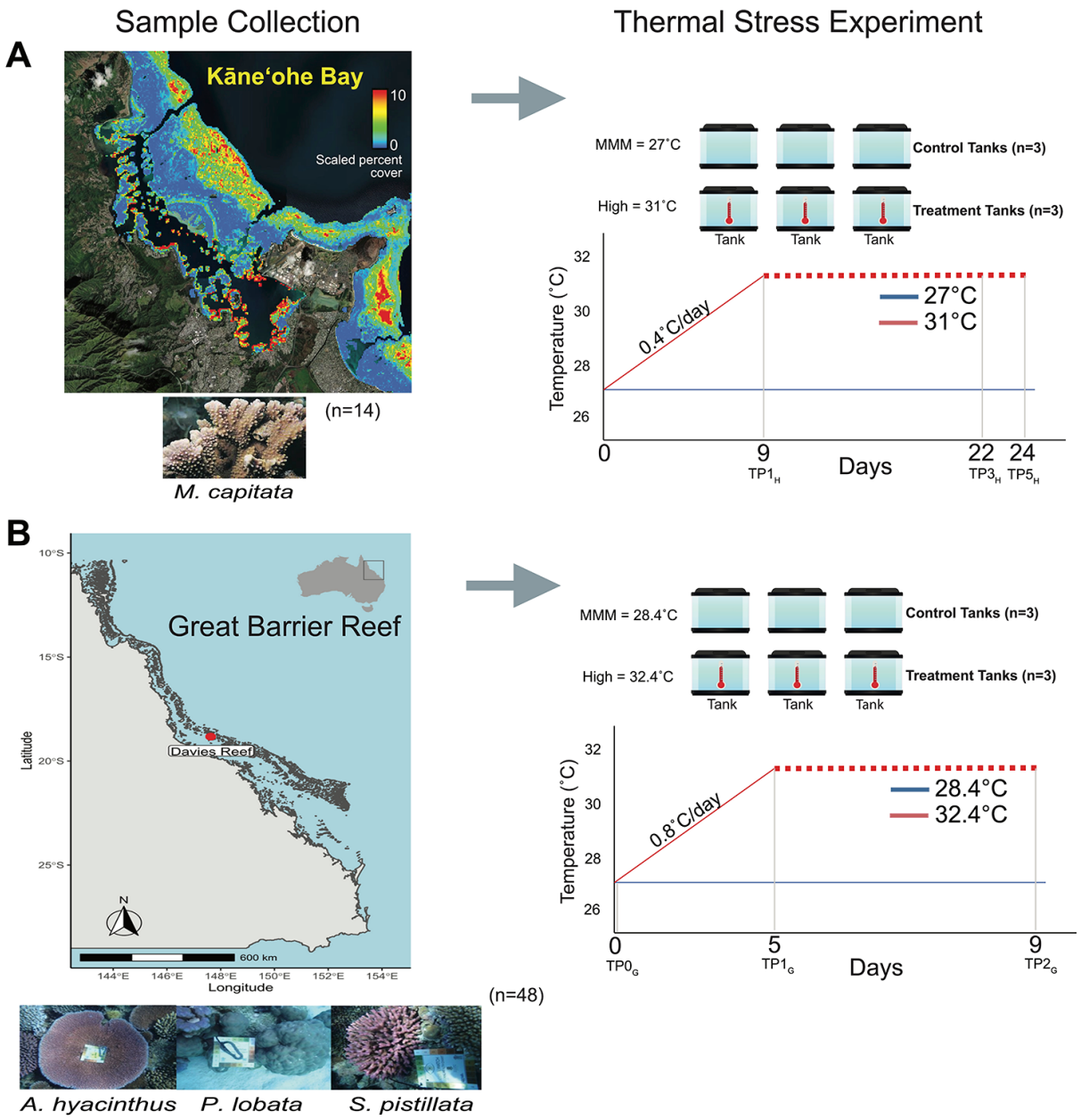
Sample Collection
Thermal Stress Experiment
A
Kāneʻohe Bay
10
0
Scaled percent cover
(n=14)
M. capitata
MMM = 27˚C
High = 31˚C
Control Tanks (n=3)
Treatment Tanks (n=3)
Tank
Tank
Tank
Temperature (˚C)
32
30
28
26
0.4˚C/day
27°C
31°C
0
9
TP1H
Days
22
24
TP3H
TP5H
B
Great Barrier Reef
Davies Reef
Latitude
10°S
15°S
20°S
25°S
N
600 km
144°E
146°E
148°E
150°E
152°E
154°E
Longitude
(n=48)
A. hyacinthus
P. lobata
S. pistillata
MMM = 28.4˚C
High = 32.4˚C
Control Tanks (n=3)
Treatment Tanks (n=3)
Tank
Tank
Tank
Temperature (˚C)
32
30
28
26
0.8˚C/day
28.4°C
32.4°C
0
TP0G
5
TP1G
Days
9
TP2G

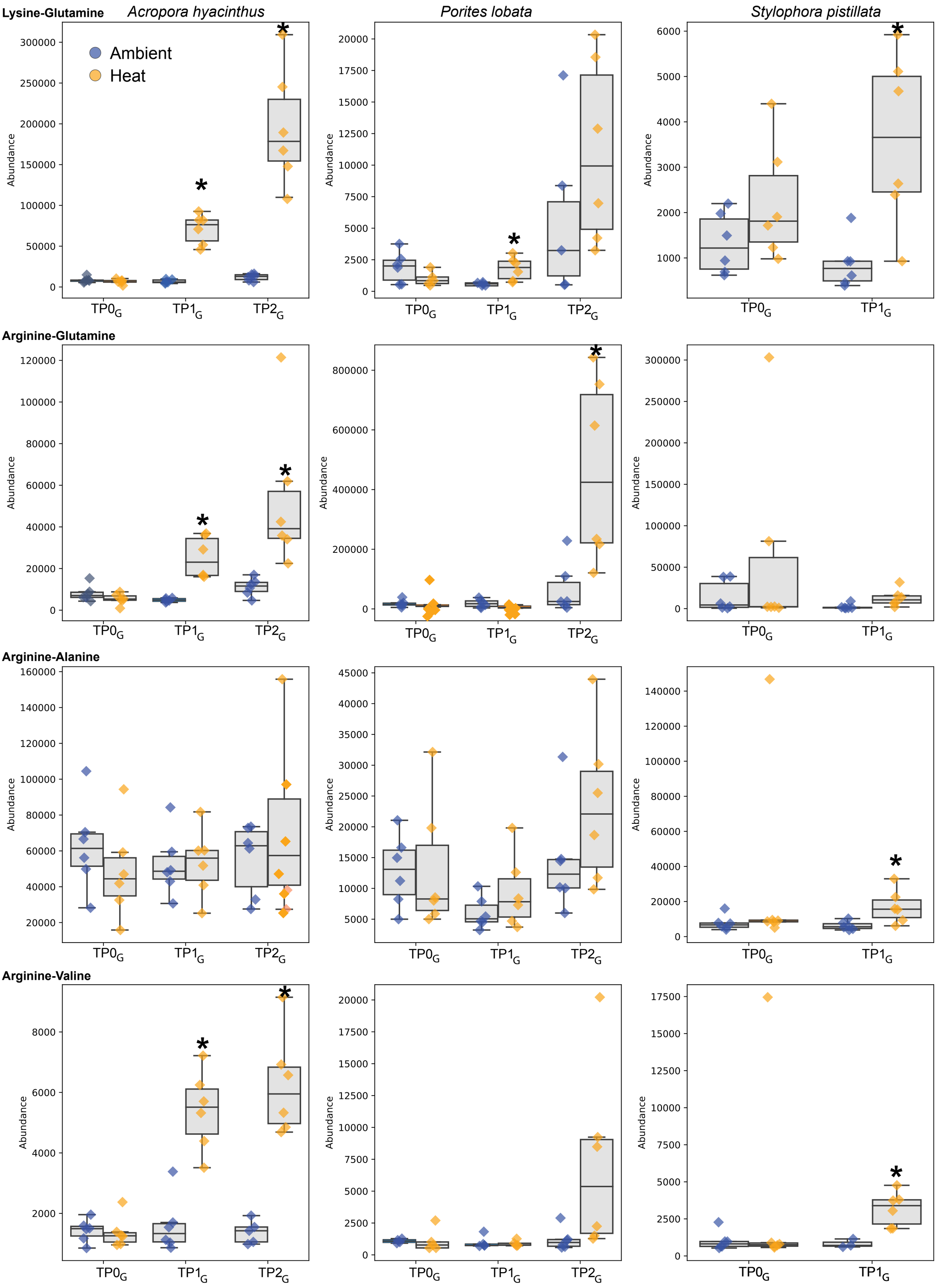
Lysine-Glutamine
Acropora hyacinthus
Porites lobata
Stylophora pistillata
Ambient
Heat
Abundance
TP0G
TP1G
TP2G
Arginine-Glutamine
Arginine-Alanine
Arginine-Valine

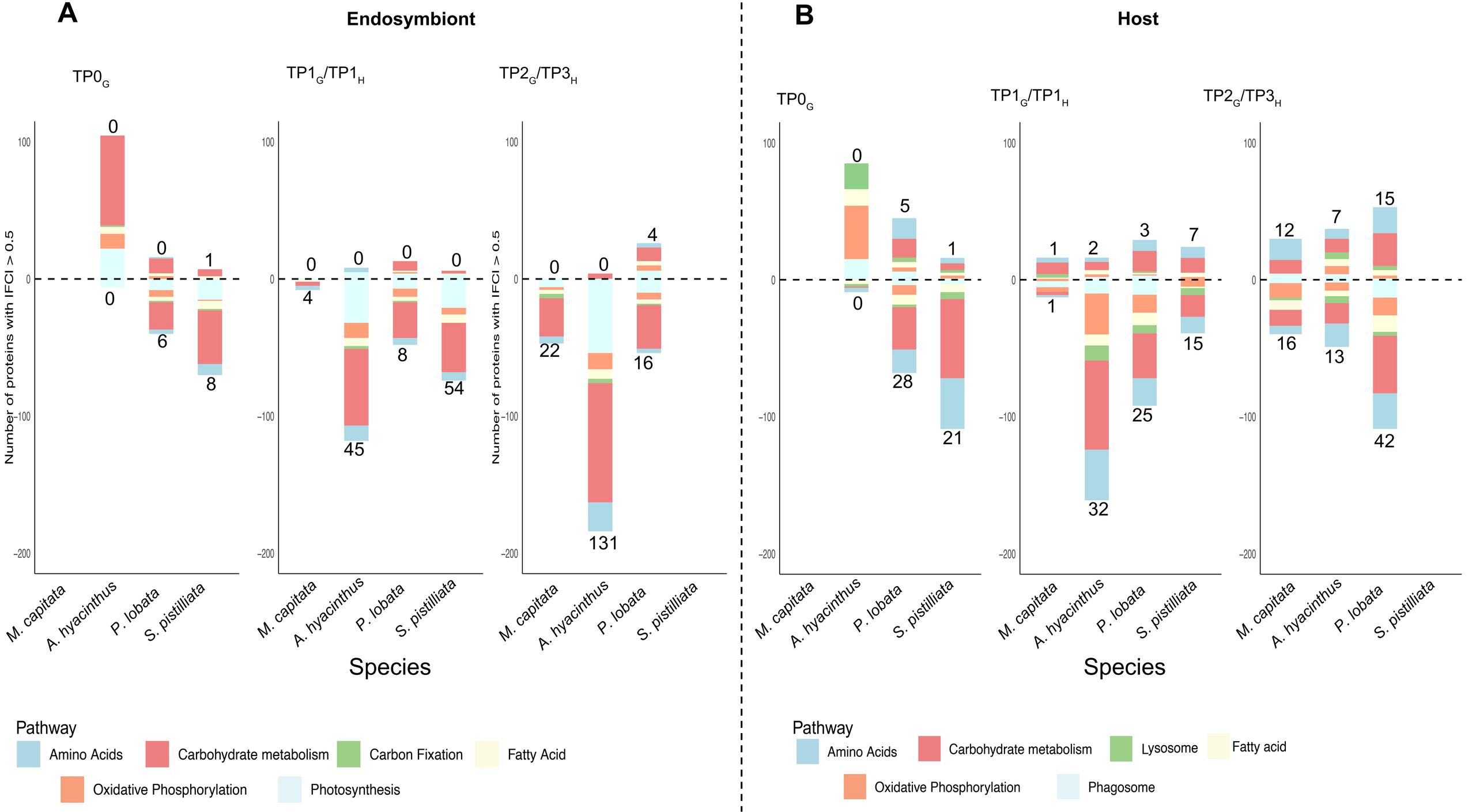
A
Endosymbiont
TP0G
TP1G/TP1H
TP2G/TP3H
Number of proteins with IFCI > 0.5
100
0
−100
−200
0
0
0
6
1
8
0
4
0
45
0
8
0
54
0
22
0
131
4
16
M. capitata
A. hyacinthus
P. lobata
S. pistilliata
Species
B
Host
TP0G
TP1G/TP1H
TP2G/TP3H
0
0
5
28
1
21
1
1
2
32
3
25
7
15
12
16
7
13
15
42
Pathway
Amino Acids
Carbohydrate metabolism
Carbon Fixation
Fatty Acid
Oxidative Phosphorylation
Photosynthesis
Pathway
Amino Acids
Carbohydrate metabolism
Lysosome
Fatty acid
Oxidative Phosphorylation
Phagosome

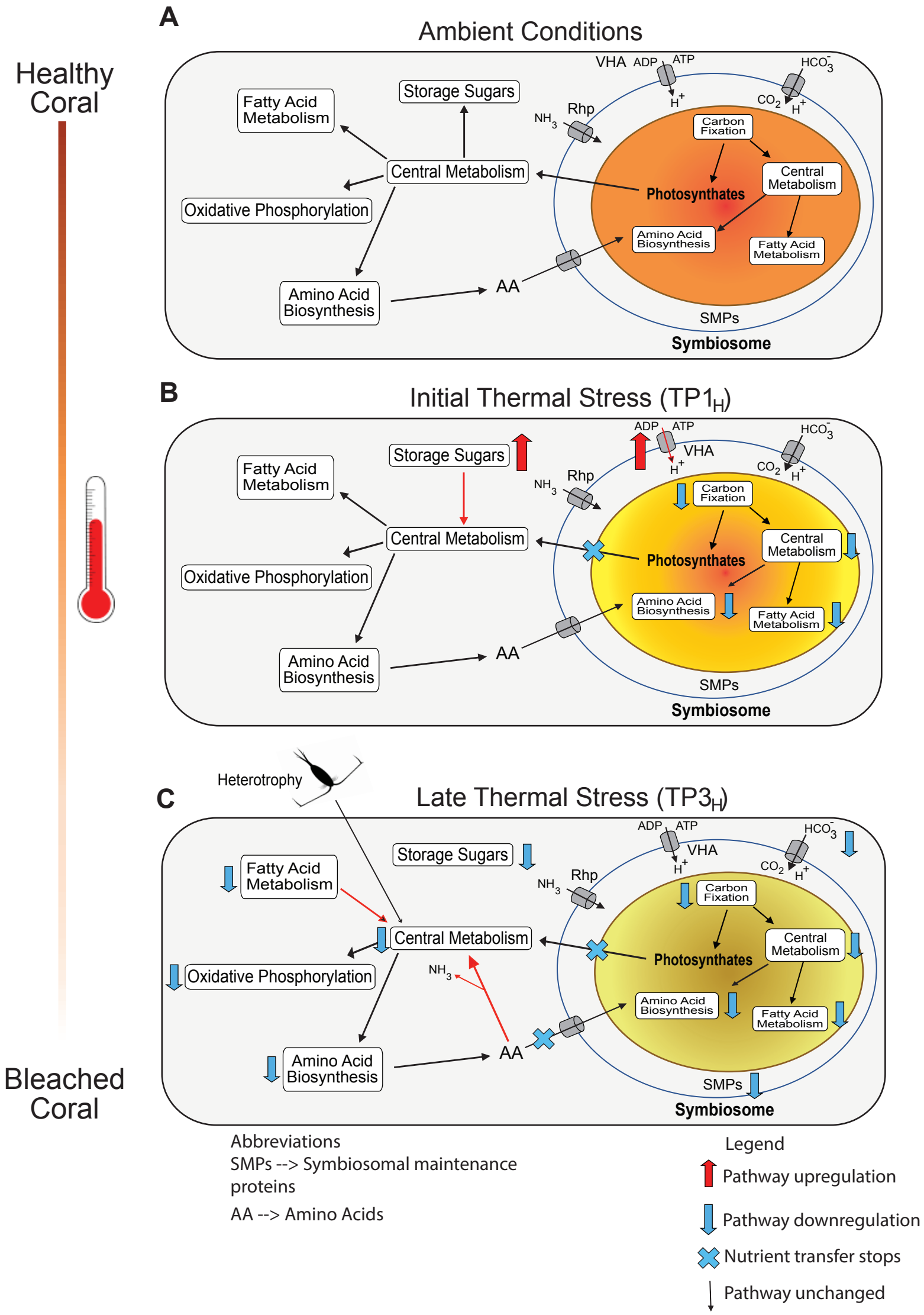
A
Ambient Conditions
Healthy Coral
Fatty Acid Metabolism
Storage Sugars
Central Metabolism
Oxidative Phosphorylation
Amino Acid Biosynthesis
AA
NH3
Rhp
VHA
ADP
ATP
H+
HCO3-
CO2
Carbon Fixation
Photosynthates
Central Metabolism
Amino Acid Biosynthesis
Fatty Acid Metabolism
SMPs
Symbiosome
B
Initial Thermal Stress (TP1H)
Storage Sugars
Fatty Acid Metabolism
Central Metabolism
Oxidative Phosphorylation
Amino Acid Biosynthesis
AA
NH3
Rhp
ADP
ATP
VHA
H+
HCO3-
CO2
Carbon Fixation
Photosynthates
Central Metabolism
Amino Acid Biosynthesis
Fatty Acid Metabolism
SMPs
Symbiosome
Heterotrophy
C
Late Thermal Stress (TP3H)
Fatty Acid Metabolism
Storage Sugars
Central Metabolism
Oxidative Phosphorylation
NH3
Amino Acid Biosynthesis
AA
NH3
Rhp
ADP
ATP
VHA
H+
HCO3-
CO2
Carbon Fixation
Photosynthates
Central Metabolism
Amino Acid Biosynthesis
Fatty Acid Metabolism
SMPs
Symbiosome
Bleached Coral
Abbreviations
SMPs --> Symbiosomal maintenance proteins
AA --> Amino Acids
Legend
Pathway upregulation
Pathway downregulation
Nutrient transfer stops
Pathway unchanged

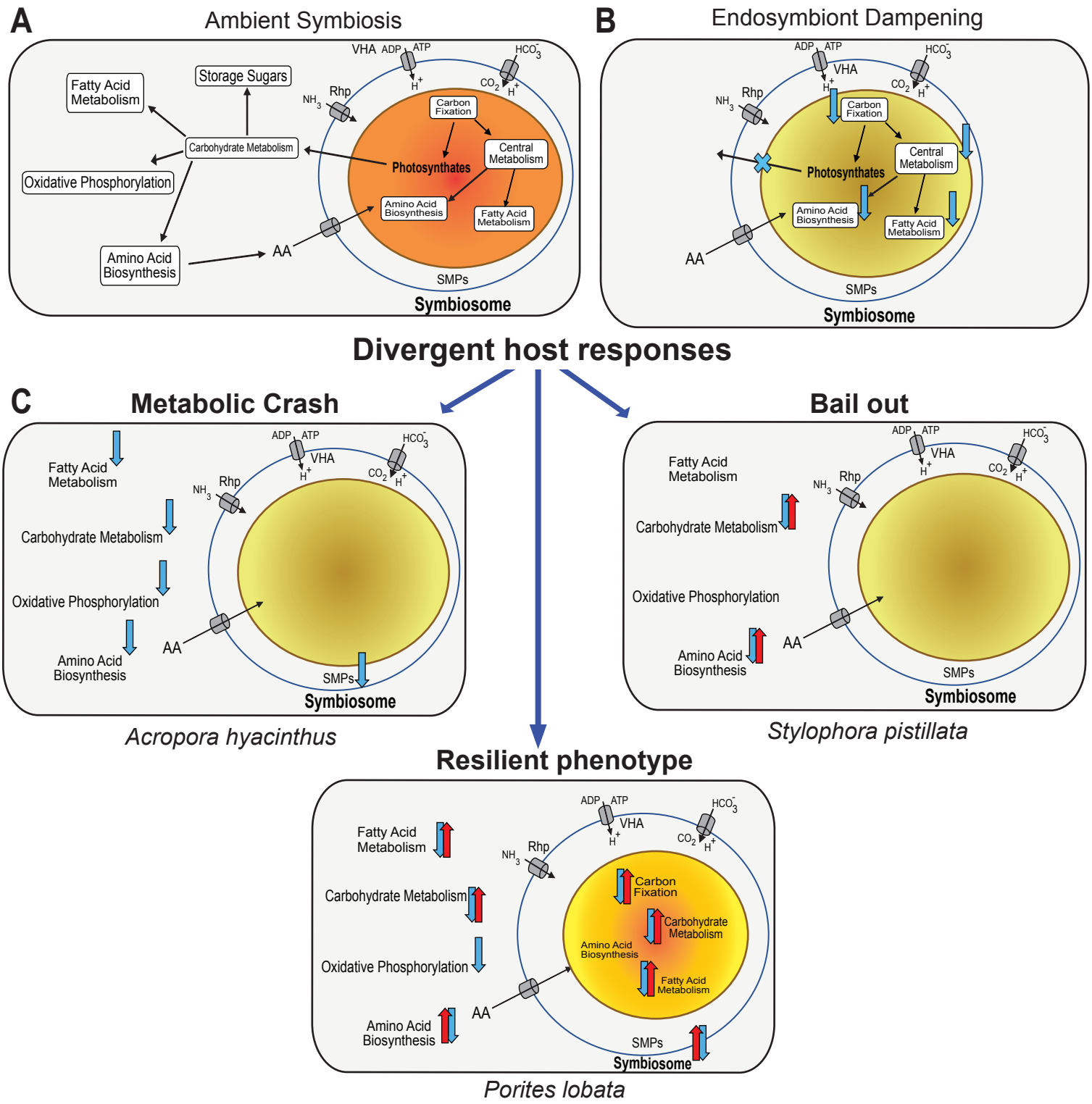
A
Ambient Symbiosis
Fatty Acid Metabolism
Storage Sugars
Carbohydrate Metabolism
Oxidative Phosphorylation
Amino Acid Biosynthesis
AA
VHA
ADP
ATP
HCO3-
NH3
Rhp
CO2
H+
Carbon Fixation
Central Metabolism
Photosynthates
Amino Acid Biosynthesis
Fatty Acid Metabolism
SMPs
Symbiosome
B
Endosymbiont Dampening
Symbiosome
Divergent host responses
C
Metabolic Crash
Fatty Acid Metabolism
Carbohydrate Metabolism
Oxidative Phosphorylation
Amino Acid Biosynthesis
Acropora hyacinthus
Bail out
Stylophora pistillata
Resilient phenotype
Porites lobata